APPLIED PHYSICS REVIEWS—FOCUSED REVIEW

Quaternary InAlGaN-based high-efficiency ultraviolet light-emitting diodes

Hideki Hirayama[a)]
The Institute of Physical and Chemical Research (RIKEN), 2-1, Hirosawa, Wako-shi, Saitama, 351-0198, Japan

(Received 17 May 2004; accepted 27 January 2005; published online 26 April 2005)

In order to realize 250–350-nm-band high-efficiency deep ultraviolet (UV) emitting devices using group-III-nitride materials, it is necessary to obtain high-efficiency UV emission from wide-band-gap (In)AlGaN. The use of the In-segregation effect, which has already been used for InGaN blue emitting devices, is quite effective for achieving high-efficiency deep UV emission. We have demonstrated high-efficiency UV emission from quaternary InAlGaN-based quantum wells in the wavelength range between 290 and 375 nm at room temperature (RT) using the In-segregation effect. Emission fluctuations in the submicron region due to In segregation were clearly observed for quaternary InAlGaN epitaxial layers. An internal quantum efficiency as high as 15% was estimated for a quaternary InAlGaN-based single quantum well at RT. Such high-efficiency UV emission can even be obtained on high threading-dislocation density buffer layers. A comparison of electroluminescence is made between light-emitting diodes (LEDs) with InAlGaN, AlGaN, and GaN active regions fabricated on SiC substrates with emission wavelengths between 340 and 360 nm. The emission intensity from the quaternary InAlGaN UV-LED was more than one order of magnitude higher than that from the AlGaN or GaN UV-LEDs under RT cw operation. We therefore fabricated 310–350-nm-band deep UV-LEDs with quaternary InAlGaN active regions. We achieved submilliwatt output power under RT pulsed operation for 308–314-nm LEDs. We also demonstrated a high output power of 7.4 mW from a 352-nm quaternary InAlGaN-based LED fabricated on a GaN substrate under RT cw operation. The maximum external quantum efficiency (EQE) of the 352-nm InAlGaN-based LED was higher than that obtained for an AlGaN-based LED with the same geometry. From these results, the advantages of the use of quaternary InAlGaN in 350-nm-band UV emitters were revealed. © *2005 American Institute of Physics*. [DOI: 10.1063/1.1899760]

TABLE OF CONTENTS

I. INTRODUCTION

AlGaN and InAlGaN alloys are attracting much attention as candidate materials for realizing deep-ultraviolet (UV) light-emitting diodes (LEDs) or laser diodes (LDs). Figure 1 shows the relationship between the direct-transition band-gap energy and the lattice constant of the wurtzite (WU) InAlGaN material system and the lasing wavelengths of various gas lasers. The direct-transition emission of AlGaN-based materials can be adjusted between 6.2 eV (AlN) and 3.4 eV (GaN). The wide emission range in the UV of (In)AlGaN covers the lasing wavelengths of various gases or solid-state UV lasers, including XeCl (308 nm) or KrF (248 nm) excimer lasers, N_2 lasers (337 nm), and He–Cd (325 nm) or Ar–second harmonic generation (SHG) (257 nm) lasers. The shortest wavelength ever achieved for group-III-nitride LEDs is 250 nm at present. However, the efficiencies of these UV-LEDs are still quite low for wavelengths shorter than 350 nm. Thus, the potential for developing UV emitting devices using (In)AlGaN alloys to realize practical applications is still considered to be very wide, as shown in Fig. 1.

Semiconductor light sources operating in the UV region are required for a number of applications, including long-lifetime white lighting, sterilization and decontamination, for use in the medical field, in biochemical processes, for the purification of the environment, and for high-density optical storage.[1,2] They are also very important for household air cleaners, automobile exhaust purifiers, UV sensing systems, and so on. Fluorescent lamps could be replaced by long-

[a)]FAX: (+81)-48-462-4659; electronic mail: hirayama@riken.jp

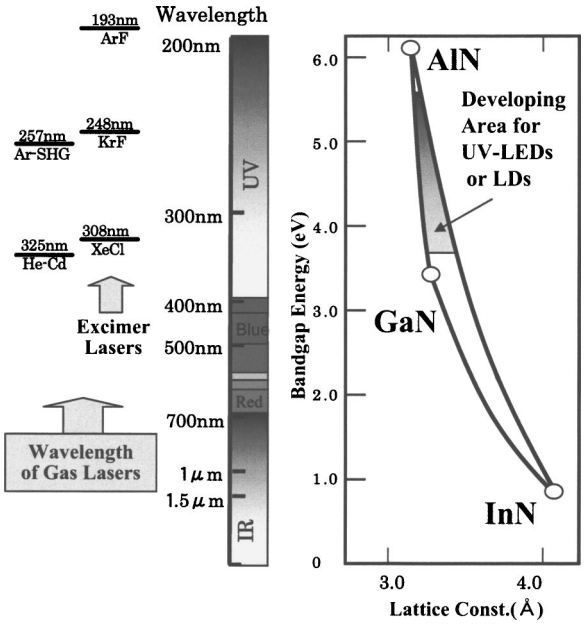

FIG. 1. Relationship between the direct-transition energy band gap and the lattice constant of wurtzite (WU) InAlGaN material and the lasing wavelengths of gas lasers.

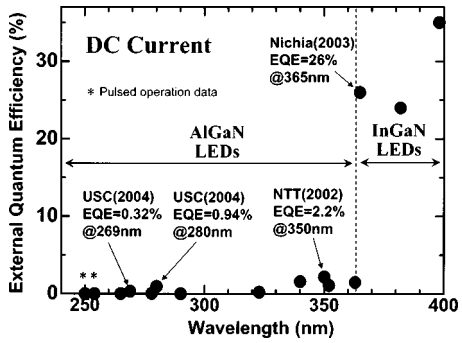

FIG. 2. Recent progress on the external quantum efficiency (EQE) of UV-LEDs at wavelengths shorter than 400 nm under room temperature (RT) cw operation.

lifetime white lamps excited by UV-LED arrays if low-cost, efficient UV-LEDs could be achieved.[1] In order to obtain high absorption efficiency of the phosphor used in white lighting, a wavelength below 350 nm is required. Efficient UV lights have also recently attracted considerable attention for the purification of the environment, i.e., the purification of river water, industrial waste water, or atmospheric gases. It has been pointed out that an efficient 280–320-nm UV light source is required for the photocatalytic decomposition of refractory pollutants (dioxin, polychlorinated biphenyls (PCB) or NO_x gas, etc.) with titanium oxide (TiO_2), or for sterilization and decontamination.[1]

The advent of solid-state UV devices has been predicted for many years. Research into the growth of single-crystal nitride-based materials with the aim of realizing blue or UV emitting devices was facilitated by Akasaki *et al.* at the end of 1960s.[3] During the 1980s, the research into group-III-nitride devices was accelerated by the several important breakthroughs, such as the realization of the high-quality single-crystal GaN,[4] the realization of *p*-type conductivity,[5] and the operation of a GaN LED.[5] An efficient UV-LED using an AlGaN/GaN double heterostructure (DH) had already been reported in 1992 by Akasaki *et al.*[6]

In order to obtain high-intensity UV emission at shorter wavelengths than can be realized by using InGaN and GaN, the development of AlGaN or quaternary InAlGaN-based UV emitters is necessary. Research into AlGaN-based UV-LEDs for wavelengths shorter than 350 nm was facilitated by several research groups between 1996 and 1998. UV-LEDs with wavelengths between 330 and 355 nm (Refs. 7–10) have been reported using AlGaN-based structures. However, their output power was still low, due to a number of technical problems.

Figure 2 summarizes the recent progress on the external quantum efficiency (EQE) of UV-LEDs at wavelengths shorter than 400 nm under room temperature (RT) cw operation. Recently, high-power near-UV LEDs at a wavelength of 365 nm have been realized by Nichia, who use InGaN in the emitting regions.[11] EQEs as high as 30% and more than 1-W output power have already been achieved at 365 nm (Ref. 12) using an InGaN active region. On the other hand, for the deep-UV wavelength range below 350 nm, various groups around the world are still trying to develop growth, fabrication techniques, and substrates, in an attempt to achieve shorter-wavelength operation while at the same time improving the output power and extraction efficiency of their devices.

In the US, this effort is being coordinated by DARPA's semiconductor ultraviolet optical sources (SUVOS) program. Innovations developed by Asif Khan and co-workers at the University of South Carolina (USC) have led to recent advances in deep-UV LEDs. They reported 250–340-nm LEDs between 2000 and 2004.[13–29] They achieved 340–305-nm InAlGaN-based LEDs in 2000 and 2001,[27–29] 325-nm AlGaN-based LEDs in 2002,[25,26] 280-nm-band AlGaN-based LEDs in 2002 and 2003,[17–24] and 250–270-nm-band AlGaN-based LEDs in 2004.[13–16] They have achieved the shortest wavelength (250 nm) for a group-III-nitride UV-LED with a single-peaked spectrum under pulsed operation.[13] They have also achieved sub-300-nm LEDs with record power and efficiency, i.e., a 280-nm, 5.2-mW LED with a maximum EQE of 0.94%,[17] and a 269-nm, 0.85-mW LED with a maximum EQE of 0.32%,[16] both under RT cw operation. They introduced micropixel design in order to improve the output power of 254- (Ref. 14) and 280-nm (Ref. 15) LEDs. Razeghi and co-workers at the Northwestern University also achieved high-power 265–340-nm deep-UV LEDs with AlGaN-based emitting layers between 2002 and 2004.[30–33] In order to achieve high-efficiency deep-UV LEDs that are useful for solid-state lightings, improvements in Al(Ga)N buffers on sapphire substrates or the use of high-quality AlN substrates are considered to be quite important. There have been several reports covering the improvement of AlGaN buffer layers, i.e., the fabrication of low-stress, crack-free, and low threading-dislocation density (TDD) Al(Ga)N buffers on sapphire,[34–38] supported by the SUVOS program. Various attempts to use high-quality AlN substrates for deep-UV emitters have also been reported.[39–41] Recently, in order to obtain high extraction efficiency of UV light, UV-LEDs with photonic crystal (PC) have been proposed, and higher extrac-

tion efficiencies have already been achieved.[42,43] Moreover, a lot of research work is presently being undertaken in an attempt to produce commercial UV-LED products such as solid-state white lighting[44–52] and UV-LED-based biosensors,[53] as well as for the development of growth and growth systems for UV-LEDs,[54–57] and so on, which is supported by many research groups and the SUVOS program.

Nishida *et al.* of NTT developed high-efficiency 340–350-nm-band UV-LEDs in the period between 1999 and 2003.[58–62] They achieved 10-mW output power at 351 nm from an AlGaN-based quantum well (QW) LED fabricated on a low-TDD GaN substrate.[58] They have also fabricated AlGaN-based LEDs on AlN/sapphire templates in order to extract UV light efficiently from the backside of the wafer, and have obtained a maximum EQE of 2.2%,[62] which is obtained for 350-nm-band nitride-based LEDs. High-efficiency AlGaN-based UV-LEDs have also been developed by the Meijo University group. They achieved efficient 363-nm LEDs by introducing low-TDD AlGaN buffer layers fabricated with the epitaxial lateral overgrowth (ELO) method.[63,64]

However, the realization of high-efficiency UV-LEDs with wavelengths below 360 nm is still challenging, as shown in Fig. 2. The maximum EQE of UV-LEDs with wavelengths shorter than 340 nm is still below 1%. It is still considered to be difficult to obtain high-efficiency 300-nm-band deep-UV LEDs for high-power solid-state lighting or another applications. The major problems in producing high-efficiency UV emitters based on group-III nitrides are summarized below. (1) It is difficult to obtain efficient UV emission at RT from AlGaN fabricated on high-TDD buffer layers or substrates. (2) It is difficult to obtain sufficient high *p*-type conductivity for the operation of UV-LED for high-Al-content AlGaN. (3) High-quality AlN substrates or low-TDD ($<1\times10^7$ cm^{-2}) AlGaN buffer layers on sapphire substrates are still difficult to fabricate.

The use of quaternary InAlGaN emitting layers is considered to be quite effective for the realization of high-efficiency UV-LEDs or laser diodes (LDs) using group-III nitrides due to the efficient emission they exhibit at wavelengths shorter than 360 nm, which is attributed to In-segregation effects. We proposed the use of quaternary InAlGaN for deep-UV emitters in 1999.[65] It is considered that the emission from a localized electron-hole pair in the In-segregation region in quaternary InAlGaN is quite effective for the purpose of obtaining bright UV emission at RT. It has been reported that the quantum-dot-like region[66,67] formed by In segregation in InGaN QWs is very effective for the suppression of nonradiative recombination and that an InGaN QW exhibits efficient emission at RT.[68,69] A similar effect to that obtained in InGaN QWs is expected for quaternary InAlGaN. Due to this effect, quaternary InAlGaN is very promising for use as the active layer of 300–350-nm-band LDs or LEDs. We have demonstrated that the intensity of the 320–340-nm UV photoluminescence (PL) from quaternary InAlGaN is as strong as that of the 430-nm blue emission from InGaN at RT.[70] We have already demonstrated high-efficiency UV emission from quaternary QWs of $In_{x1}Al_{y1}Ga_{1-x1-y1}N/In_{x2}Al_{y2}Ga_{1-x2-y2}N$ in the wavelength range between 300 and 350 nm at RT (Ref. 71) and efficient 308–352-nm InAlGaN-based UV-LEDs.[72–77] The growth and optical properties of quaternary InAlGaN have also been investigated by groups in the US and elsewhere, including the growth of quaternary InAlGaN using a pulsed gas supply,[78,79] band-gap engineering, the basic optical properties and localized carrier effects of quaternary InAlGaN alloys,[80–84] and investigations into the mechanism of high-efficiency UV emission based on a piezoelectric field.[85,86] Quaternary InAlGaN emitting regions have been introduced by many research groups in order to achieve high-efficiency operation for 305–370-nm UV-LEDs.[27–29,87,88]

The most important advantage of the use of quaternary InAlGaN is that the UV emission intensity is not so sensitive to the TDD, as has been previously clarified for InGaN-based emitters. It has been reported that threading dislocations act as nonradiative centers in the GaN layer.[89] These results have been confirmed by studies using transmission electron microscopy (TEM) and cathodoluminescence (CL).[90] In general, the edge dislocations from the majority of the total line defects density in group-III-nitride layers grown by metal-organic chemical-vapor deposition (MOCVD).[91] Correlations between line defects (edge, screw, and mixed dislocations) and the optical properties have been carefully investigated by Miyajima *et al.*[91] They confirmed that screw and mixed dislocations act as strong nonradiative centers in GaN and InGaN layers. They also showed that not only screw and mixed dislocations but also edge dislocations become nonradiative centers.[91] The emission intensity of AlGaN and GaN epitaxial layers is very sensitive to the dislocation density, as confirmed in Ref. 63. Therefore, UV devices using AlGaN-based active regions need to be fabricated on low-TDD buffers or substrates. On the other hand, quaternary InAlGaN UV-LEDs show high-efficiency operation, even when fabricated on high-TDD buffer layers, as shown later. The use of quaternary InAlGaN is particularly important for UV emitters, since high-quality AlN substrates or low-TDD AlGaN buffer layers on sapphire substrates are still difficult to achieve.

The purpose of this work is to realize 300–350-nm-band high-efficiency UV-LEDs. In this paper, we will describe the detailed emitting properties of AlGaN and quaternary InAlGaN, and show techniques for the realization of high-efficiency 300–350-nm-band quaternary InAlGaN-based UV-LEDs. In Sec. II, we describe the growth and optical properties of high-Al-content $Al_xGa_{1-x}N$ for application to deep-UV emitters. The growth conditions for high-quality $Al_xGa_{1-x}N$ are investigated and a single-peak spectrum from high-Al-content $Al_xGa_{1-x}N$ (Al content up to 80%) is observed emitting from near the band edge. Intense UV emission around 230–280 nm is demonstrated from $Al_xGa_{1-x}N/Al_yGa_{1-y}N$ multiquantum wells (MQWs) with wide-band-gap AlGaN barriers. The intensity of the deep-UV emission from AlGaN-based MQWs is shown to be as high as that of the blue emission from InGaN-based QWs at 77 K. However, the 200-nm-band UV emission from AlGaN-based QWs at RT is much weaker than the blue emission from InGaN.

In Sec. III, we describe the growth and the optical prop-

erties of quaternary $In_xAl_yGa_{1-x-y}N$ to obtain intense UV emission at RT by using the In-segregation effect. We reveal that efficient RT emission can be obtained from $In_{x1}Al_{y1}Ga_{1-x1-y1}N/In_{x2}Al_{y2}Ga_{1-x2-y2}N$ QWs in the wavelength range between 290 and 375 nm. The UV emission from quaternary InAlGaN is shown to be as strong as the blue emission from InGaN at RT.

In Sec. IV, we describe UV-LEDs with InAlGaN emitting regions. We demonstrate submilliwatt output power under RT pulsed operation from 308 to 314 nm quaternary InAlGaN-based LEDs fabricated on sapphire substrates. We also fabricated quaternary InAlGaN QW LEDs on GaN substrates in order to eliminate the effects of TDD. We demonstrate an output power of 7.4 mW at a wavelength of 352 nm under RT cw operation. We also demonstrate the EQE for 350-nm-band UV-LEDs with top-emission geometry. From these results, we will confirm the advantages of using the quaternary InAlGaN for 300–350-nm-band UV-emitting devices.

Finally, in Sec. V, we summarize this work and discuss possible future developments.

II. GROWTH AND OPTICAL PROPERTIES OF $Al_xGa_{1-x}N$

In this section, we describe how we investigated the basic growth conditions and optical properties of AlGaN as a first step to developing quaternary InAlGaN with efficient UV emission at RT. We demonstrate efficient UV PL at wavelengths ranging from 230 to 280 nm from $Al_xGa_{1-x}N(AlN)/Al_yGa_{1-y}N$ MQWs grown on SiC by metal-organic vapor phase epitaxy (MOVPE).[92,93] We systematically investigated the PL intensity of AlGaN-based MQWs as functions of both the QW thickness and the Al content of the barriers.[94,95] The efficiency of the deep-UV emission from AlGaN-based QWs is shown to be as high as that of the blue emission from InGaN-based QWs at 77 K.

The samples were grown at 76 Torr on the Si face of an on-axis 6H-SiC (0001) substrate, using a conventional horizontal-type MOVPE system. Ammonia (NH_3), trimethylaluminum (TMAl), and trimethylgallium (TMGa) were used as precursors, with H_2 as the carrier gas. N_2 gas was supplied independently by a separate line in order to control the gas flow. Typical gas flows were 2, 2, and 0.5 SLM for NH_3, H_2, and N_2, respectively. The molar fluxes of TMGa and TMAl for the growth of $Al_xGa_{1-x}N$ ($x=0.11$–1) were 3.8–38 and 2.6–45 μmol/min, respectively. Under these conditions, the growth rates of $Al_{0.11}Ga_{0.89}N$, $Al_{0.40}Ga_{0.60}N$, and AlN were approximately 2.4, 1.0, and 0.4 μm/h, respectively. The substrate temperature during the growth of the $Al_xGa_{1-x}N$, as measured using a thermocouple located at the substrate susceptor, was approximately 1140, 1170, and 1200 °C for Al contents (x) of 10%–40%, 40%–80%, and 80%–100%, respectively. All of the samples were undoped. The molar fraction x of Al in the $Al_xGa_{1-x}N$ alloy was determined by four-crystal x-ray diffraction (XRD) measurements.

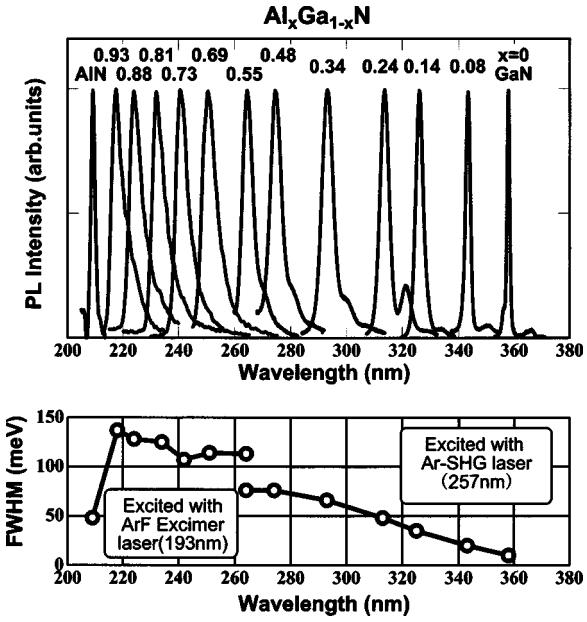

FIG. 3. Spectra and full width at half maximum (FWHM) of the PL emission observed from the $Al_xGa_{1-x}N$ alloy over the entire AlN compositional range measured at 77 K.

We investigated the optical properties of the $Al_xGa_{1-x}N$ alloy over the entire AlN compositional range, i.e., GaN to AlN. Figure 3 shows the spectra and full width at half maximum (FWHM) of the PL emission observed from the $Al_xGa_{1-x}N$ alloy over the entire AlN compositional range at 77 K. We observed single-peaked PL spectra from near the band edge over the entire Al compositional range. The yellow emission around 500–550 nm was negligible, even for high-Al-content AlGaN. The phonon-replica peaks seen at the low-energy side of each spectrum for Al contents of 0.11–0.53 confirm the high crystalline quality of the AlGaN. Typical values of FWHM of the PL spectrum at 77 K were approximately 20, 65, and 100 meV for Al contents of 10%–20%, 35%–60%, and 70%–95%, respectively. We observed PL emission from AlN (208 nm) from near the band edge.

We then fabricated four series of AlGaN MQW samples, consisting of $Al_xGa_{1-x}N$ barriers with different Al contents. Table I summarizes the structure and the thickness of the buffer, barrier, and well layers and the PL peak wavelength range of each series of AlGaN MQWs. Figure 4 shows an

TABLE I. Structure and thickness of the buffer, barrier, and quantum-well layers, displayed with the PL peak-wavelength range of each series of AlGaN MQWs.

Sample series	Structure	Buffer (thickness) (nm)	Barrier (thickness) (nm)	Well (thickness) (nm)	Peak wavelength (nm)
(a)	5-MQW on 6H-SiC	AlN (250)	AlN (5)	$Al_{0.18}Ga_{0.82}N$ (1.2–3.3)	229–285
(b)	···	$Al_{0.8}Ga_{0.2}N$ (250)	$Al_{0.8}Ga_{0.2}N$ (5)	$Al_{0.18}Ga_{0.82}N$ (1.3–3.3)	238–288
(c)	···	$Al_{0.7}Ga_{0.3}N$ (300)	$Al_{0.7}Ga_{0.3}N$ (5)	$Al_{0.12}Ga_{0.88}N$ (1.4–2.7)	255–303
(d)	···	$Al_{0.53}Ga_{0.47}N$ (400)	$Al_{0.53}Ga_{0.47}N$ (5)	$Al_{0.11}Ga_{0.89}N$ (1.4–3.4)	272–343

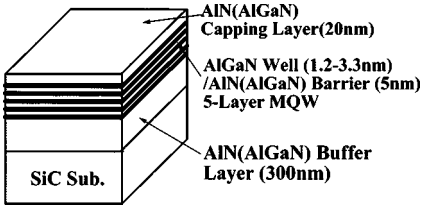

FIG. 4. Schematic layer structure of the fabricated $AlN/Al_{0.18}Ga_{0.82}N$ MQW sample.

example of the schematic layer structure of an AlN/AlGaN five-layer MQW sample [sample series (a) in Table I]. In order to achieve a flat surface suitable for the growth of AlGaN QWs, an approximately 250–400-nm-thick AlN(AlGaN) buffer layer was deposited, followed by a very thin AlN layer on a SiC wafer. We confirmed a step-flow-grown surface by atomic force microscopy (AFM) for each series of samples. The threading-dislocation density (TDD) of the AlGaN buffer was approximately 1×10^{10} cm^{-2}.[96] As the next step, a five-layer MQW consisting of 1.2–3.4-nm-thick $Al_xGa_{1-x}N$ wells ($x=0.11$–0.18), 5–nm-thick $Al_yGa_{1-y}N$ barriers ($y=0.53$–1), and a 10-nm-thick $Al_yGa_{1-y}N$ cap ($y=0.53$–1) was grown. The well and barrier thicknesses were simply estimated from the growth rate of the bulk AlGaN or AlN.

Figure 5 shows the PL spectra of (a) $AlN/Al_{0.18}Ga_{0.82}N$, (b) $Al_{0.80}Ga_{0.20}N/Al_{0.18}Ga_{0.82}N$, (c) $Al_{0.70}Ga_{0.30}N/Al_{0.12}Ga_{0.88}N$, and (d) $Al_{0.53}Ga_{0.47}N/Al_{0.12}Ga_{0.88}N$ five-layer MQWs for various well thicknesses. The samples were excited at 77 K using a Xe-lamp light source (215 nm) for sample series (a) and (b), a Xe-lamp light source (227 nm) for sample series (c), and an Ar-SHG laser (257 nm) for sample series (d). The excitation power densities with the Xe-lamp source and the Ar-SHG laser were approximately 20 W/cm^2 and 5 kW/cm^2, respectively. We obtained a single-peak intense PL emission from every MQW. No yellow emission was observed from any of the samples. The most efficient emission was obtained at wavelengths of 234, 245, 255, and 282 nm for sample series (a), (b), (c), and (d), respectively. The optimum value for the well thickness was approximately 1.5 nm for each series of samples. The PL spectra of bulk $Al_{0.80}Ga_{0.20}N$ and bulk $Al_{0.53}Ga_{0.47}N$ (thickness approximately 400 nm) are also shown in Figs. 5(b) and 5(d), respectively, as references. The PL intensity of the MQWs was 20–30 times larger than that of the bulk AlGaN, due to a quantized confinement effect. A quantized energy-level shift can be clearly observed, as seen in Figs. 5(a)–5(d). The PL peak energies for different well thicknesses agree well with the calculated levels of the quantized energies, taking into account the piezoelectric field applied in the QW regions. The values of the piezoelectric field in the well regions, as estimated from the positions of the measured quantized levels, are more than 2 MV/cm, as already pointed out by Bernardini *et al.*.[97] The PL intensity depends heavily on the well thickness. A rapid reduction in the PL intensity with increasing well thickness was seen for each series of samples. The reason for this is considered to be a reduction of the radiative recombination probability due to the large piezoelectric field in the well.[98] The reduction of the emission intensity when the well is thinner than 1.5 nm may be due to an increase in the nonradiative recombination on the heterointerfaces.

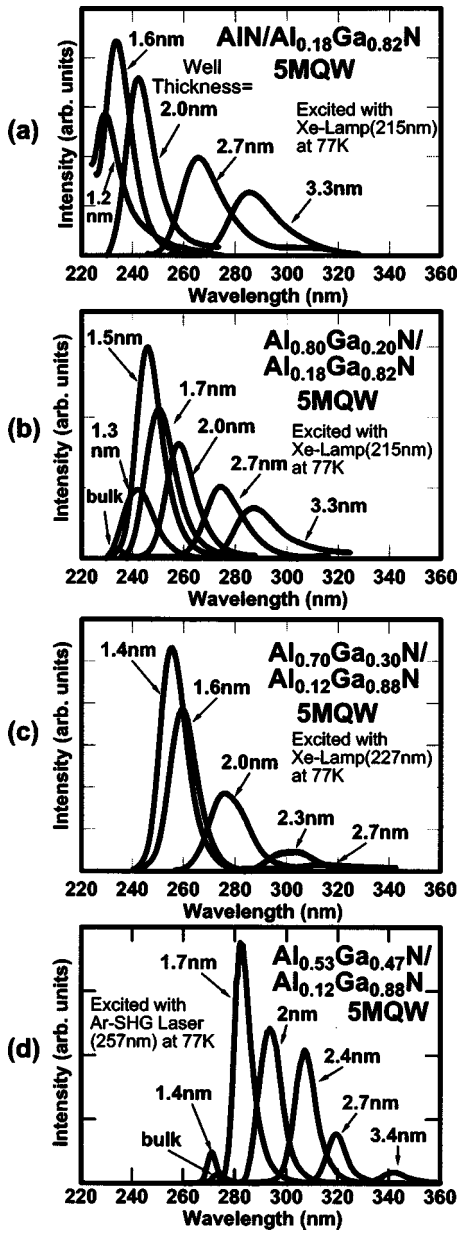

FIG. 5. PL spectra of (a) $AlN/Al_{0.18}Ga_{0.82}N$, (b) $Al_{0.80}Ga_{0.20}N/Al_{0.18}Ga_{0.82}N$, (c) $Al_{0.70}Ga_{0.30}N/Al_{0.12}Ga_{0.88}N$, and (d) $Al_{0.53}Ga_{0.47}N/Al_{0.12}Ga_{0.88}N$ five-layer MQWs for various well thicknesses.

Figure 6 shows a comparison of the PL intensity among AlGaN-, GaN-, and InGaN-based QWs with optimized QW structures, as measured at 77 K. All of the samples were excited with a Xe-lamp light source (215 nm) under the same excitation conditions. We found that the PL intensity of the 234-nm emission from an $AlN/Al_{0.18}Ga_{0.82}N$ MQW is as strong as that of the 420-nm emission from an $In_{0.02}Ga_{0.98}N/In_{0.20}Ga_{0.80}N$ single quantum well (SQW), and is much stronger than that from an $Al_{0.12}Ga_{0.88}N/GaN$ MQW at 77 K. This result indicates that the AlGaN-based QW structure is grown with atomically flat heterointerfaces, even when the Al content of the AlGaN barrier is very high. However, the emissions from the AlGaN- and GaN-based QWs at

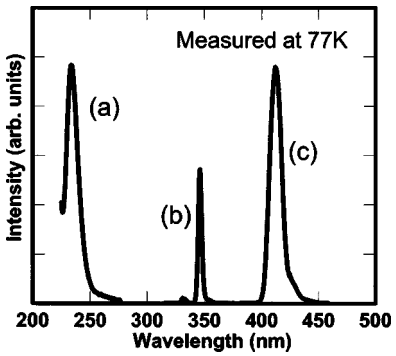

FIG. 6. Comparison of PL intensity between (a)AlN/$Al_{0.18}Ga_{0.82}N$ five-layer MQW, (b)$Al_{0.11}Ga_{0.89}N$/GaN five-layer MQW, and (c) $In_{0.02}Ga_{0.98}N/In_{0.2}Ga_{0.8}N$ SQW with optimized QW structures at 77 K.

room temperature are much weaker compared with the emissions from InGaN-based QWs. The emission from InGaN-based QWs is even efficient at room temperature,[68,69] due to a high ratio of radiative recombination from localized carriers in the In-segregation regions. These In-segregation effects can also be applicable to InAlGaN-based QWs. The emission of AlGaN-based QWs may be significantly increased by the incorporation of a small amount of In at room temperature. Also, by reducing the threading-dislocation density on the AlGaN buffer, the emission intensity of the AlGaN-based QWs at room temperature may be greatly increased.

In summary, in this section we have demonstrated single-peak PL spectra from near the band edge of $Al_xGa_{1-x}N$ over the entire Al compositional range. We systematically investigated the PL intensity of $Al_xGa_{1-x}N(AlN)/Al_yGa_{1-y}N$ MQWs with wide-band-gap AlGaN barriers as functions of the QW thickness and the Al content of the barriers. Single-peak efficient PL emission was obtained between 282 and 234 nm at 77 K by changing the Al content of the $Al_xGa_{1-x}N$ barriers from 53% to 100%. The efficiency of the deep-UV emission from AlGaN-based QWs was as high as that of the blue emission from InGaN-based QWs at 77 K.

III. GROWTH AND CHARACTERIZATION OF QUATERNARY $In_xAl_yGa_{1-x-y}N$ FOR UV EMITTERS

The emissions from AlGaN-based structures were found to be very efficient at low temperature, as described in the Sec. II: however, they were weak at RT when fabricated on high-TDD (1×10^{10} cm^{-2}) AlGaN buffers. Therefore, AlGaN-based structure grown on a usual high-TDD buffer is difficult to use as an emitting layer in a high-efficiency UV device. We proposed the use of In segregation in quaternary InAlGaN for the purpose of obtaining RT bright UV emission.[65] It has been reported that the emission from localized carriers in the In-segregation region in InGaN QWs is very efficient, with the suppression of nonradiative recombination.[68,69] The In-segregated region will be less effective for confining electron-hole pairs at higher temperature. The strong emission from InGaN in comparison with that from AlGaN is considered to be due to that the carriers captured into the In-rich region recombine radiatively before being trapped in the nonradiative centers generated by defects. A similar effect to that obtained in InGaN QWs is expected for quaternary InAlGaN. Due to this effect, quaternary InAlGaN is very promising for use as the active layer of 300–350-nm-band LDs or LEDs. Quaternary InAlGaN has previously been used for the fabrication of unstrained QW systems grown on GaN or AlGaN buffer layers, rather than for the fabrication of UV emitters. In this case, the possible emission wavelength range of the QWs is around 370–380 nm in order to satisfy the lattice-matched conditions. On the other hand, we intend to use quaternary InAlGaN for the realization of much shorter-wavelength (250–350-nm-band) UV-LEDs or LDs.

In this section, we reveal systematic conditions for the growth of quaternary $In_xAl_yGa_{1-x-y}N$ emitting in the 300-nm band using MOCVD, and demonstrate strong UV emission from the $In_xAl_yGa_{1-x-y}N$-based bulk material and QWs. We reveal that UV emission is considerably enhanced by the In-segregation effect upon introducing 1%–5% of In into the AlGaN. Indium incorporation in quaternary $In_xAl_yGa_{1-x-y}N$ is markedly enhanced with increasing Al content when using a relatively high growth temperature (830–850 °C), resulting in efficient RT UV emission.[70] We demonstrate intense RT emission in the wavelength range between 290 and 380 nm from quaternary $In_xAl_yGa_{1-x-y}N$-based MQWs.[71]

The samples were grown on the Si face of on-axis 6H-SiC (0001) substrates by MOVPE. Layer structures consisting of $In_xGa_{1-x}N$ or quaternary $In_xAl_yGa_{1-x-y}N$ were grown on an approximately 400-nm-thick $Al_xGa_{1-x}N$ ($x=0.12$–0.4) buffer layer to achieve a flat surface that was suitable for the QW layer. The threading-dislocation density of the AlGaN buffer was approximately 1×10^{10} cm^{-2}.[96] The precursors and the growth conditions used for AlGaN growth were the same as those mentioned in the preceding section. Trimethylindium di-isopropylamine-adduct ($[(CH_3)_3]In(i\text{-}C_3H_7)_2NH$; TMI-adduct) was used as the indium source. The growth conditions for quaternary InAlGaN were based on the InGaN growth condition. Typical gas flows used for In(Al)GaN were 2 and 1.5 SLM for NH_3 and N_2, respectively. The molar fluxes of TMGa, TMAl, and TMI-adduct for the growth of $In_xGa_{1-x}N$ or quaternary $In_xAl_yGa_{1-x-y}N$ were 1.5, 0.13–0.78, and 30 μmol/min, respectively. Typical growth temperatures for the $In_xGa_{1-x}N$ and quaternary $In_xAl_yGa_{1-x-y}N$ were 750–780 °C and 800–870 °C, respectively. Under these conditions, the typical growth rates of the $In_xGa_{1-x}N$ and of the quaternary $In_xAl_yGa_{1-x-y}N$ were 0.1 and 0.12 μm/h, respectively. The optical properties of the InGaN and the quaternary InAlGaN films were investigated by PL measurements with excitation from an Ar-SHG laser (257.3 nm). The excitation power density was approximately 5 kW/cm^2.

First, we fabricated undoped $In_xAl_yGa_{1-x-y}N$ films on 400-nm-thick $Al_{0.12}Ga_{0.88}N$ buffer layers. Figure 7 shows the PL spectra of 120-nm-thick quaternary $In_xAl_yGa_{1-x-y}N$ for various TMAl flow rates measured at 77 K. The PL spectrum of 120-nm-thick InGaN is also shown for reference. All the samples were grown at 830 °C, which is approximately 50–80 °C higher than the growth temperatures used for $In_xGa_{1-x}N$($x=0.2$–0.4). As observed in Fig. 7, the emission from InGaN grown at 830 °C is weak because of the small

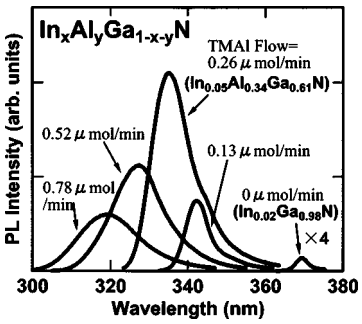

FIG. 7. PL spectra of 120-nm-thick $In_{0.02}Ga_{0.98}N$ and quaternary $In_xAl_yGa_{1-x-y}N$ for various TMAl flow rates grown at 830 °C, measured at 77 K.

amount of In incorporation (approximately 2%) due to the relatively high growth temperature for InGaN. On the other hand, the emission is markedly enhanced by increasing the TMAl flow rate. This emission enhancement is due to an increase in the In content in the quaternary $In_xAl_yGa_{1-x-y}N$, which is markedly increased with increasing molar flux of Al. The In content (x) of the $In_xGa_{1-x}N$ was 2.2% and the In and Al contents (x) and (y) of the quaternary $In_xAl_yGa_{1-x-y}N$ for a TMAl flow rate of 0.26 μmol/min were 4.8% and 34%, respectively, as measured by Rutherford backscattering spectrometry (RBS). The tendencies of the growth conditions obtained in our quaternary InAlGaN growth agree well with the analytical deposition diagrams that have been calculated for the MOVPE growth of quaternary InAlGaN by Koukitu *et al.*, based on a thermodynamic analysis.[99] The emission intensity of $In_{0.05}Al_{0.34}Ga_{0.61}N$ at 77 K and RT was as strong as that of $In_{0.2}Ga_{0.8}N$ with the same film thickness. The marked enhancement in the emission intensity in quaternary InAlGaN is considered to be mainly due to the effect of In segregation, which was already observed for the InGaN alloy.

Figures 8(a)–8(d) show ω-2θ scan profiles (0002) of the XRD rocking curves measured using a four-crystal XRD measurement system that were obtained for the $In_{0.022}Ga_{0.978}N$ and quaternary $In_xAl_yGa_{1-x-y}N$ samples with various TMAl flow rates that were used for the PL measurements in Fig. 7. The peaks at around θ=17.85° and 17.4° that appear in each profile correspond to the diffractions from the 6H-SiC (0001) substrate and the $Al_{0.12}Ga_{0.88}N$ buffer layer, respectively. As is observed in Figs. 8(a)–8(d), the quaternary $In_xAl_yGa_{1-x-y}N$ peak shifts from θ =17.3°–17.7° with an increasing TMAl flow rate between 0 and 0.78 μmol/min. Typical values of the full width at half maximum (FWHM) of the XRD rocking curves for the quaternary $In_xAl_yGa_{1-x-y}N$ were approximately 200 s, which were almost the same values obtained for $In_{0.022}Ga_{0.978}N$.

Figure 9 shows the PL spectra of 120-nm-thick quaternary $In_xAl_yGa_{1-x-y}N$ for various In flow rates measured at 77 K. The PL spectrum of 120-nm-thick $Al_{0.2}Ga_{0.8}N$ is also shown for reference. All of the samples were also grown at 830 °C. The In contents (x) in the quaternary $In_xAl_yGa_{1-x-y}N$ were approximately 2% and 5% for TMI-adduct flow rates of 3 and 30 μmol/min, respectively, as determined by RBS measurements. The small emission peak at around 342 nm in each spectrum is the emission from the $Al_{0.12}Ga_{0.88}N$ buffer layers. The emission from the reference $Al_{0.2}Ga_{0.8}N$ film is

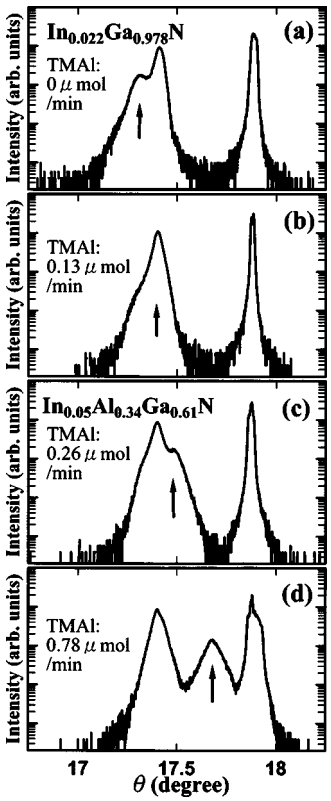

FIG. 8. ω-2θ scan profiles (0002) of the x-ray diffraction (XRD) rocking curves obtained for $In_{0.022}Ga_{0.978}N$ and quaternary $In_xAl_yGa_{1-x-y}N$ with various TMAl flow rates measured by the four-crystal XRD measurement system.

weak because the layer is thin. We found that the emission intensity of AlGaN is markedly enhanced by incorporating approximately 2%–5% of In. We hypothesize that this is mainly due to a marked reduction in nonradiative recombination due to the effects of In segregation, as shown later. We can observe several emission peaks in the spectrum obtained for a TMI-adduct flow rate of 3 μmol/min, which are considered to be due to compositional phase separation in the quaternary $In_xAl_yGa_{1-x-y}N$. Moreover, the crystalline quality is improved by incorporating In into the AlGaN; this is confirmed by XRD measurements.

Figure 10 shows a cathodoluminescence (CL) image from a 600-nm-thick $In_{0.034}Al_{0.121}Ga_{0.845}N$ layer measured at

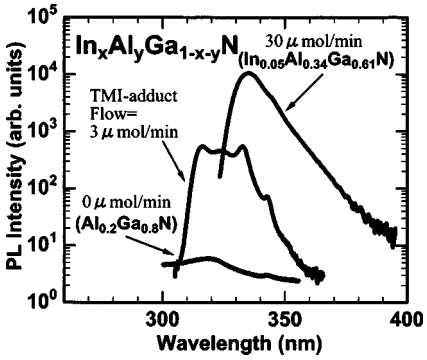

FIG. 9. PL spectra of 120-nm-thick $Al_{0.2}Ga_{0.8}N$ and quaternary $In_xAl_yGa_{1-x-y}N$ for various TMI-adduct flow rates grown at 830 °C, measured at 77 K.

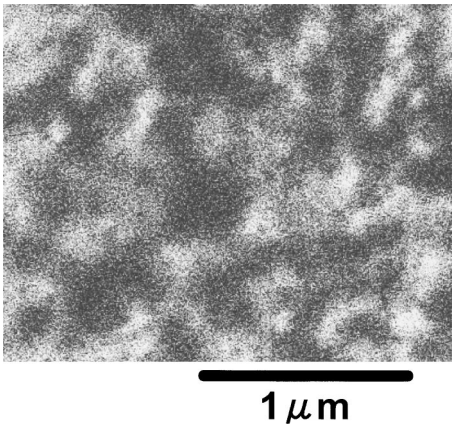

FIG. 10. Cathodoluminescence (CL) image from 600-nm-thick quaternary $In_{0.034}Al_{0.121}Ga_{0.845}N$ measured at around 110 K.

around 110 K. The CL image was measured at around the peak energy of the spectrum (355 nm). Emission fluctuations in the submicron region were clearly observed in the CL image. The emission fluctuation is considered to be due to carrier localization in the In-segregation area. We obtained similar CL images for quaternary $In_xAl_yGa_{1-x-y}N$ with different In and Al compositions emitting at 315–370 nm. The CL images obtained for quaternary InAlGaN films were very similar to those obtained for InGaN films.

Figure 11 shows the PL spectra measured at RT of $In_{0.22}Ga_{0.78}N$ and quaternary $In_xAl_yGa_{1-x-y}N$ with different In and Al compositions ($x=1.3\%-4.4\%$, $y=12.0\%-31.2\%$). We used the optimized growth temperature and TMAl flow rate to obtain the maximum PL intensity for each emission wavelength in the growth of both the InGaN and quaternary InAlGaN layers. The growth temperatures of the InGaN or quaternary InAlGaN used for samples (a)–(e) in Fig. 11 were 770, 790, 810, 830, and 870 °C, respectively. We found that the appropriate growth temperature for quaternary InAlGaN is higher than that for InGaN by 40–100 °C in order to obtain intense 300-nm-band UV PL. The required growth temperature becomes higher as the emission wavelength becomes shorter for quaternary InAlGaN. We obtained intense PL emission from quaternary InAlGaN in the wavelength range between 315 and 370 nm at RT. The PL intensity of the UV emission from quaternary InAlGaN was as large as that of the blue emission from InGaN at RT. These results indicate that quaternary InAlGaN is very promising for use as the active layer of QWs for 300–360-nm-band UV-LDs or bright LEDs.

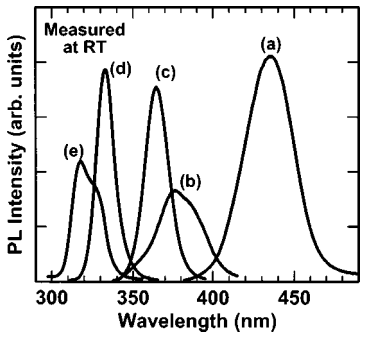

FIG. 11. PL spectra of (a) $In_{0.22}Ga_{0.78}N$, (b) $In_{0.044}Al_{0.120}Ga_{0.836}N$, (c) $In_{0.034}Al_{0.121}Ga_{0.845}N$, (d) $In_{0.020}Al_{0.275}Ga_{0.705}N$, and (e) $In_{0.013}Al_{0.312}Ga_{0.675}N$ grown on SiC, all with thickness of 120 nm, measured at RT.

We then fabricated InAlGaN-based QWs on SiC. We investigated well the thickness dependencies of the PL property for six series of In(Al)GaN-based QWs with various In and Al compositional ranges in In(Al)GaN. Table II summarizes the structure of the QWs, the compositional wavelengths of the quaternary InAlGaN and the InGaN used for the wells and barriers, the optimized well thicknesses for obtaining intense PL, and the emission wavelength range of intense PL.

Figure 12 shows an example of the schematic layer structure of an InAlGaN MQW fabricated on a SiC substrate [which corresponds to series (b) in Table II and Fig. 13(b)]. The structure consists of a 400-nm-thick $Al_{0.15}Ga_{0.85}N$ buffer layer grown on SiC, a 50-nm-thick $In_{0.02}Al_{0.60}Ga_{0.38}N$ buffer region with a thin (approximately 3 nm) $In_{0.05}Al_{0.34}Ga_{0.61}N$ strain reduction layer, an $In_{0.05}Al_{0.34}Ga_{0.61}N/In_{0.02}Al_{0.60}Ga_{0.38}N$ three-layer MQW, and a 20-nm-thick $In_{0.02}Al_{0.60}Ga_{0.38}N$ cap. The barrier thickness was fixed at 7 nm. The QW thickness was changed from 0.7 to 3.5 nm. All of the layers were undoped.

Figure 13 shows the PL spectra of (a) $In_{0.03}Al_{0.50}Ga_{0.47}N/In_{0.01}Al_{0.60}Ga_{0.39}N$ three-layer MQWs, (b) $In_{0.05}Al_{0.34}Ga_{0.61}N/In_{0.02}Al_{0.60}Ga_{0.38}N$ three-layer MQWs, (c) $In_{0.06}Al_{0.08}Ga_{0.86}N/In_{0.02}Al_{0.52}Ga_{0.46}N$ three-layer MQWs, (d) $In_{0.06}Al_{0.09}Ga_{0.85}N/In_{0.03}Al_{0.18}Ga_{0.79}N$ SQWs, (e) $In_{0.15}Ga_{0.85}N/In_{0.02}Al_{0.15}Ga_{0.83}N$ three-layer MQWs, and (f) $In_{0.20}Ga_{0.80}N/In_{0.02}Ga_{0.98}N$ SQWs for various well thicknesses. All samples were excited at RT with an Ar-SHG laser (257 nm). In order to make a strict comparison of the PL intensity between the samples, the excitation power of the Ar-SHG laser were stabilized to maintain the same value. The values of In and Al compositions of quaternary

TABLE II. Structures, compositional wavelengths of the InAlGaN and InGaN used for the wells and barriers, the optimized well thicknesses, and the wavelength range of intense emission of each series of fabricated In(Al)GaN/In(Al)GaN QWs.

Sample series	QW structure (well / barrier)	Compositional wavelength (well) (nm)	Compositional wavelength (barrier) (nm)	Optimized well thickness (nm)	Wavelength range of intense emission (nm)
(a)	InAlGaN/InAlGaN-3MQW	308	270	2.1	290–313
(b)	InAlGaN/InAlGaN-3MQW	340	300	1.4	318–338
(c)	InAlGaN/InAlGaN-3MQW	364	310	2.1	325–355
(d)	InAlGaN/InAlGaN-SQW	362	345	1.5	358–375
(e)	InGaN/InAlGaN-3MQW	408	334	(3.3)	370–395
(f)	InGaN/InGaN-SQW	430	370	2.8	405–448

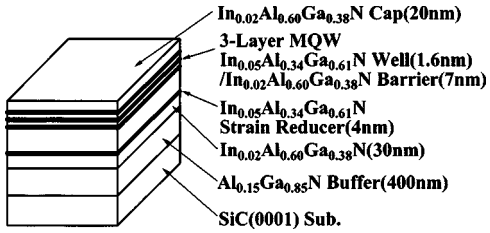

FIG. 12. Schematic of the layer structure of an $In_{0.05}Al_{0.34}Ga_{0.61}N/In_{0.02}Al_{0.60}Ga_{0.38}N$ three-layer MQW grown on a SiC wafer.

InAlGaN indicated in Figs. 13(a)–13(e) were estimated from the RBS measurement, PL peak wavelength, and growth conditions, i.e., growth temperature and the fluxes of the group-III gases. We obtained a single-peaked intense PL emission from every MQW. The most efficient emission was obtained at wavelengths of 300, 318, 338, 357, 395, and 428 nm for sample series (a), (b), (c), (d), (e), and (f), respectively. The optimum value for the well thickness was 1.5–3 nm. The PL intensity of the MQWs was more than ten times larger than that of the bulk InAlGaN, due to a quantized confinement effect. A quantized energy-level shift can be clearly seen, as seen in Figs. 13(a)–13(f). The PL intensity depends heavily on the well thickness. A reduction in the PL intensity with increasing well thickness was seen for each series of samples except for (e). The reason for this is considered to be a reduction of the recombination probability due to the generation of higher-order hole-quantized levels or due to the effect of piezoelectric field in the well. The piezoelectric field in an InAlGaN-based QW has been reported to be much smaller than that observed in an InGaN-based QW from the investigation of the optical properties under high pressure.[85,86] The reduction of the emission intensity when the well is thinner than 1.5 nm may be due to an increase in the nonradiative recombination on the heterointerfaces. For QW sample series (e), the strong PL was not obtained for thin (around 2 nm) quantum well. The reason for this is that the crystalline quality of quaternary InAlGaN barrier was not sufficiently high, as discussed later.

Figure 14 shows a comparison at RT between the UV emission spectra obtained from quaternary InAlGaN QWs and a blue emission spectrum obtained from an InGaN QW, all with optimized quantum well thicknesses. The spectra (a)–(f) in Fig. 14 correspond to series (a)–(f) in Table II and Figs. 13(a)–13(f). We obtained 290–375-nm intense UV emission from InAlGaN-based QWs at RT. The intensity of the 320–360-nm UV emission from quaternary InAlGaN QWs is as strong as that of the blue emission from InGaN QWs at RT. The emission intensity at RT is weak for wavelengths below 280 nm. This is because a higher growth temperature was used to maintain the high crystalline quality of quaternary InAlGaN with high Al content, and thus the incorporation of In into the InAlGaN quaternary was reduced due to the high growth temperature. When the In incorporation in quaternary InAlGaN is smaller than 1%, the emission intensity at RT is much reduced, because of the reduction of the effect of In compositional fluctuation. The emission intensity of the InGaN/InAlGaN QWs of wavelength at 380–400 nm is also not strong, as seen in Fig. 14(e), in comparison with the blue emission from InGaN-based QWs. This is thought to be caused by the degradation of the crystalline quality of quaternary InAlGaN barrier layers due to the use of a relatively low growth temperature, which is required to increase In incorporation into InGaN well. As discussed above, higher growth temperature used for InGaN growth is required to obtain sufficiently high crystalline quality of quaternary InAlGaN. If higher growth temperature is used only

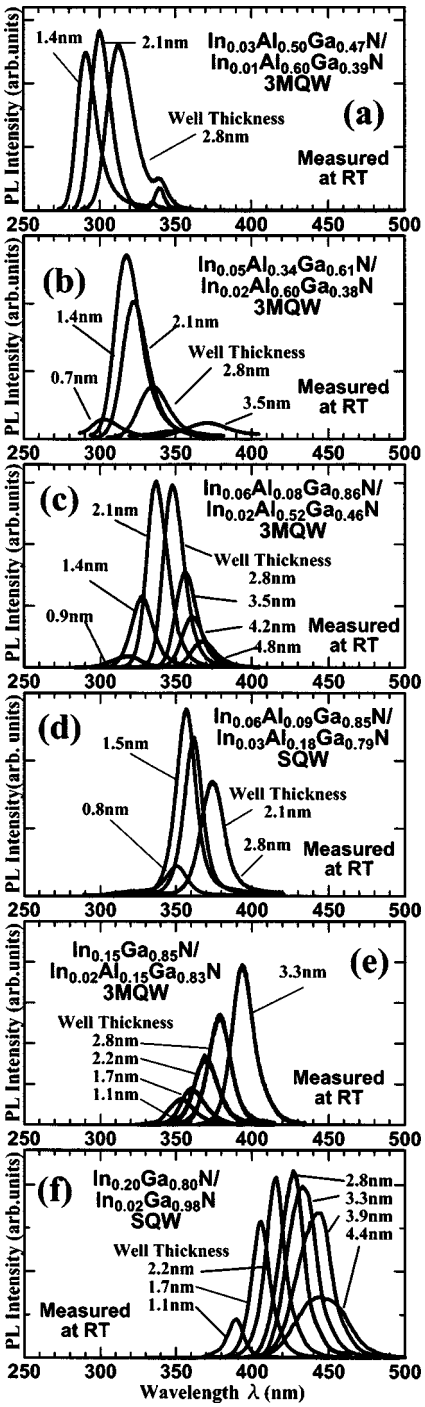

FIG. 13. PL spectra of (a) $In_{0.03}Al_{0.50}Ga_{0.47}N/In_{0.01}Al_{0.60}Ga_{0.39}N$ three-layer MQWs, (b) $In_{0.05}Al_{0.34}Ga_{0.61}N/In_{0.02}Al_{0.60}Ga_{0.38}N$ three-layer MQWs, (c) $In_{0.06}Al_{0.08}Ga_{0.86}N/In_{0.02}Al_{0.52}Ga_{0.46}N$ three-layer MQWs, (d) $In_{0.06}Al_{0.09}Ga_{0.85}N/In_{0.03}Al_{0.18}Ga_{0.79}N$ SQWs, (e) $In_{0.15}Ga_{0.85}N/In_{0.02}Al_{0.15}Ga_{0.83}N$ three-layer MQWs, and (f) $In_{0.20}Ga_{0.80}N/In_{0.02}Ga_{0.98}N$ SQWs for various well thicknesses measured at RT.

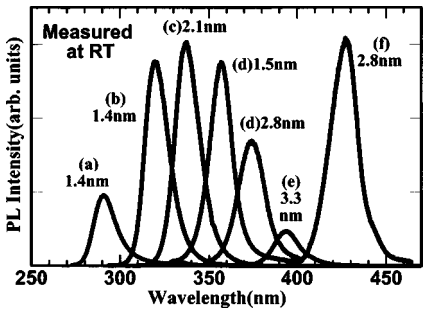

FIG. 14. Comparison of PL emission intensity between the 300-nm-band UV emission obtained from quaternary InAlGaN-based QWs and the blue emission obtained from an InGaN-based QW, with optimized quantum well thicknesses.

for InAlGaN barrier layers, the emission intensity may be much higher.

Figure 15 shows the temperature dependences of the PL intensity of an $In_{0.05}Al_{0.34}Ga_{0.61}N/In_{0.02}Al_{0.60}Ga_{0.38}N$ three-layer MQW, an $In_{0.20}Ga_{0.80}N/In_{0.02}Ga_{0.98}N$ SQW, a $GaN/Al_{0.15}Ga_{0.85}N$ five-layer MQW, and an $Al_{0.12}Ga_{0.88}N/Al_{0.53}Ga_{0.47}N$ five-layer MQW with optimized QW thicknesses. The PL intensity of each sample is normalized to the PL intensity obtained at 20 K. As seen in Fig. 15, the temperature dependence of the PL emission for InAlGaN-based QWs was greatly improved in comparison with that of GaN- or AlGaN-based QWs. The PL intensity of InAlGaN and InGaN-based QWs was one to two orders of magnitude higher than that of GaN- or AlGaN-based QWs at RT. The RT emission efficiency of the QWs was considered to be markedly improved due to the increase in radiative recombination caused by the localized electron-hole pairs in the In-segregation region, as indicated by CL measurements.

Figure 16 shows the temperature dependence of the PL intensity of InAlGaN-based SQW grown on SiC [sample series (d) in Table II]. The emission peak wavelength at RT and well thickness of the SQW sample were 357 and 1.5 nm, respectively. The internal quantum efficiency (IQE) was estimated from the ratio of the PL intensity measured at low temperature (10 K) and at RT. The estimated value of the IQE was approximately 15% at RT. The threading-

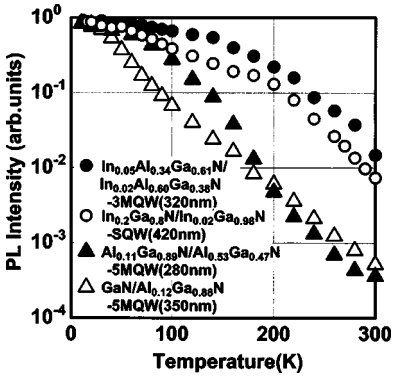

FIG. 15. Temperature dependences of PL intensity of an $In_{0.05}Al_{0.34}Ga_{0.61}N/In_{0.02}Al_{0.60}Ga_{0.38}N$ three-layer MQW, an $In_{0.20}Ga_{0.80}N/In_{0.02}Ga_{0.98}N$ SQW, a $GaN/Al_{0.15}Ga_{0.85}N$ five-layer MQW, and an $Al_{0.12}Ga_{0.88}N/Al_{0.53}Ga_{0.47}N$ five-layer MQW with optimized QW thicknesses.

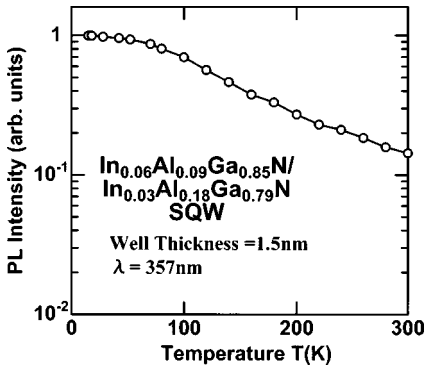

FIG. 16. Temperature dependence of the PL intensity of InAlGaN-based SQW grown on SiC [sample series (d) in Table II].

dislocation density (TDD) measured by a high-resolution scanning electron microscope[95] (HR-SEM) on an InAlGaN epitaxial layer on SiC was as high as 1×10^{10} cm^{-2}. On AlGaN buffer layers with such a high density of TDs, the IQE of AlGaN- or GaN-based QWs is quite low. This high EQE value estimated for InAlGaN-based QWs is thought to be due to In-segregation effects.

To summarize this section, we demonstrated intense UV emission at RT from quaternary $In_xAl_yGa_{1-x-y}N$ alloys grown by MOVPE. We found that the UV emission is considerably enhanced by the In-segregation effect upon introducing 2%–5% of In into the AlGaN. The incorporation of In into quaternary $In_xAl_yGa_{1-x-y}N$ is markedly enhanced by increasing the Al content when using a relatively high growth temperature (830–850 °C), resulting in efficient RT UV emission. Maximum emission efficiency was obtained at around 320–360 nm from the fabricated quaternary $In_xAl_yGa_{1-x-y}N$ (where $x=2.0\%$–3.4%, $y=12\%$–28%). The intensity of the 330-nm emission from quaternary $In_{0.034}Al_{0.12}Ga_{0.85}N$ was as strong as that of the 430-nm emission from $In_{0.22}Ga_{0.78}N$ at RT. We clearly observed In segregation on a submicron scale from CL images of quaternary InAlGaN films. We also demonstrated intense UV emission at RT in the wavelength range between 290 and 375 nm for $In_{x1}(Al_{y1})Ga_{1-x1-y1}N/In_{x2}Al_{y2}Ga_{1-x2-y2}N$ MQWs. The temperature dependence of the PL emission for InAlGaN-based QWs was greatly improved in comparison with that of GaN- or AlGaN-based QWs. These results indicate that quaternary InAlGaN is very promising for use as the active layer of 300–350-nm-band UV-LDs or bright LEDs.

IV. InAlGaN-BASED UV-LEDs

A. AlGaN- and InAlGaN-based UV-LEDs on SiC

In this subsection, we describe AlGaN- and InAlGaN-based UV-LEDs emitting at wavelengths around 340 nm that were fabricated using the techniques mentioned in the preceding sections. We demonstrate high-intensity UV-LEDs using quaternary InAlGaN as the active region for wavelengths around 340 nm.[100,101] A comparison of electroluminescence (EL) is made between InAlGaN, AlGaN, and GaN LEDs fabricated on SiC substrates that emit between 340 and 360 nm.[72,100]

Figure 17 shows (a) the schematic structure and (b) the current injection spectra for various current densities of the

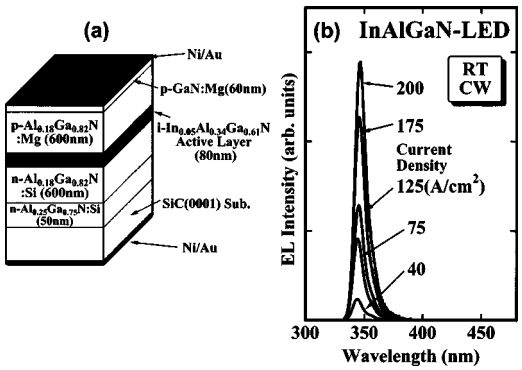

FIG. 17. (a) Schematic structure and (b) current injection spectra measured under RT cw operation of a quaternary InAlGaN UV-LED fabricated on a SiC substrate with an emission wavelength of 345 nm.

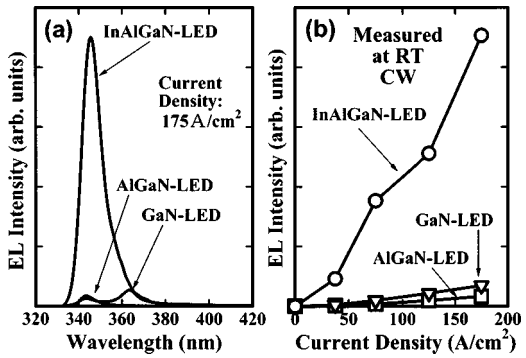

FIG. 18. Comparison of (a) emission spectra and (b) emission intensities as a function of injection current density among UV-LEDs with quaternary $In_{0.05}Al_{0.34}Ga_{0.61}N$, $Al_{0.18}Ga_{0.82}N$, and GaN active regions.

fabricated quaternary InAlGaN UV-LED. The LED structures were grown on 6H-SiC substrates. The structure consisted of a 50-nm-thick Si-doped $Al_{0.25}Ga_{0.75}N$ buffer layer, a 600-nm-thick Si-doped $Al_{0.17}Ga_{0.83}N$ layer, an 80-nm-thick undoped quaternary $In_{0.05}Al_{0.34}Ga_{0.61}N$ active layer, a 600-nm-thick Mg-doped $Al_{0.18}Ga_{0.82}N$ layer, and a 60-nm-thick Mg-doped GaN capping layer. The samples were annealed at 800 °C in a N_2 gas flow for 30 min in order to activate the Mg acceptors. The Mg incorporation in the Mg-doped $Al_{0.18}Ga_{0.82}N$ layer was approximately 1×10^{20} cm^{-3}, as determined by secondary-ion-mass spectroscopy (SIMS) measurements. The hole and electron concentrations in the Mg-doped $Al_{0.18}Ga_{0.82}N$ layer and in both the Si-doped $Al_{0.25}Ga_{0.75}N$ and the $Al_{0.15}Ga_{0.85}N$ layers were approximately 2×10^{17} and 1×10^{18} cm^{-3}, respectively, as obtained from Hall-effect measurements. Ni/Au electrodes were used for both the *p*-type surface and the *n*-type SiC substrate. The diameter of the *p*-side electrode was approximately 0.6 mm.

The emission spectra were measured under RT cw operation. The injection current density was changed within the range of 0–200 A/cm^2. We obtained single-peaked bright emission with a wavelength of 345 nm from the quaternary InAlGaN LEDs. We did not observe any deep-level emissions, such as emission from Mg-acceptor levels, nor 550-nm-band yellow emission. In addition, there was neither a significant wavelength shift nor any output power saturation with increasing injection current in the current-density range between 0- and 200 A/cm^2. The UV output power of the LED was not high because of absorption losses through the *p*-GaN cap layer and the Ni/Au *p* electrode. A high output power is expected if the structure could be optimized to extract UV light.

Figure 18 shows (a) the emission spectra and (b) the emission intensities as a function of injection current density of UV-LEDs with quaternary $In_{0.05}Al_{0.34}Ga_{0.61}N$, $Al_{0.18}Ga_{0.82}N$, and GaN as the active regions, all measured under RT cw operation. The layer structures of the AlGaN and GaN LEDs were the same as that used for the quaternary InAlGaN LED, except for the active region. As is evident from Figs. 18(a) and 18(b), the UV emission intensity from the quaternary InAlGaN LED was more than one order of magnitude larger than that from the AlGaN or GaN LEDs. The TDD of an AlGaN buffer on SiC was approximately 1×10^{10} cm^{-2}. Therefore, the use of quaternary InAlGaN as an UV emitting region is advantageous, particularly in the case where it is fabricated on a high-TDD buffer.

In summary of this subsection, we fabricated UV-LEDs on SiC substrates using a quaternary InAlGaN active region and achieved bright 345-nm emission under RT cw operation. The UV intensity from quaternary InAlGaN LEDs was more than one order of magnitude higher than that obtained from AlGaN or GaN LEDs. From these results, we revealed that the use of quaternary InAlGaN as the emitting regions of UV emitters is advantageous in comparison with AlGaN or GaN, particularly when they are fabricated on wafers with high-TDD buffer layers.

B. 310-nm-band InAlGaN LEDs on sapphire

For realizing the shorter-wavelength nitride-based LEDs or LDs, the achievement of high-quality *p*-type AlGaN with high Al content is one of the key requirements. In particular, for UV-LEDs operating in the wavelength range below 350 nm, the requirement for a sufficiently high-hole concentration in *p*-type AlGaN is important for suppressing electron overflow and for obtaining high injection efficiency. The highest possible limit of the Al content for Mg-doped $Al_xGa_{1-x}N$ is approximately 30% in order to obtain the desired hole conductivity. Recently, considerable research has been performed to realize high-hole conductivity in group-III-nitride materials, i.e., the use of superlattices (SLs)[102–105], Mg-doped InGaN (Ref. 106) or quaternary InAlGaN,[107] or codoping in GaN or AlGaN.[108]

It is difficult to obtain a sufficiently high-hole concentration in *p*-type AlGaN with a high Al content. The main reason for this is that the energy level of the Mg acceptor is deep for high-Al-content AlGaN, and thus the activated hole concentration is quite low. In order to obtain hole conductivity, heavy Mg doping of as high as 10^{21} cm^{-3} is required. Such a heavily Mg-doped AlGaN easily becomes *n* type due to an increase in the number of vacancies or defects in the crystal. Therefore, in order to obtain adequate hole conductivity for high-Al-content *p*-type AlGaN, the identification of growth conditions for obtaining high crystalline quality AlGaN for even heavy Mg doping is necessary.

We introduced an alternating gas flow growth technique for the growth of high-Al-content *p*-type AlGaN.[108] The

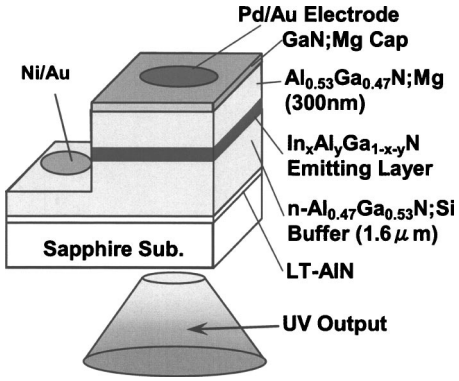

FIG. 19. Schematic structure of a quaternary InAlGaN UV-LED fabricated on a sapphire substrate with an emission wavelength of around 310 nm.

crystalline quality of high-Al-content *p*-type AlGaN is considered to be remarkably improved due to enhanced migration of the precursors when using the alternating gas flow sequence. Moreover, by using alternating gas supply, the vapor reactions between ammonia and TMAl or ammonia and the Mg source are considered to be significantly suppressed in front of the graphite susceptor. The crystalline quality of high-Al-content AlGaN is considered to be drastically improved by the suppression of these gas-phase reactions.

By growing with alternating gas flow, we achieved hole conductivity in Mg-doped AlGaN with Al contents of between 46% and 53%. On the other hand, we could not obtain *p*-type character for high-Al-content Mg-doped AlGaN grown with a conventional continuous gas flow regime. These results indicate that the alternating gas flow growth method is advantageous for obtaining high-Al-content *p*-AlGaN.

In this subsection, we describe on InAlGaN-based 310-nm-band UV-LEDs with high-Al-content *p*-type AlGaN on sapphire substrates.[74] Figure 19 shows the schematic LED structure. The layer structure consists of a low-temperature (LT)-AlN layer, a 1.6-μm-thick Si-doped $Al_xGa_{1-x}N$ ($x=0.47$) buffer layer, an approximately 60-nm-thick undoped $In_xAl_yGa_{1-x-y}N$ emitting layer, a 300-nm-thick Mg-doped $Al_xGa_{1-x}N$($x=0.53$) layer, and a 30-nm-thick Mg-doped GaN contact layer. For the growth of Mg-doped AlGaN, an alternating gas flow sequence was used. We employed a high Al content (greater than 50%) for the *p*-type AlGaN in order to suppress electron overflow adequately. If a lower-Al-content *p*-AlGaN layer was used, the LED intensity was weak, since the electron injection efficiency into the QW was low due to electron overflow.

We fabricated two types of LEDs with different emission wavelengths, i.e., 308 and 314 nm. The compositional wavelengths of the quaternary InAlGaN emitting layers of the LEDs were tuned to 308 and 314 nm. The In and Al compositions of the quaternary InAlGaN emitting regions were approximately 0.02 and 0.46, and 0.02 and 0.42, respectively, for emission wavelengths of 308 and 314 nm. The UV emission could be extracted from the backside of the sapphire substrate through the *n*-$Al_{0.47}Ga_{0.53}N$ layer below the InAlGaN emitting layer, as shown in Fig. 19. The samples were annealed at 830 °C in a nitrogen atmosphere for 40 min in order to activate the Mg acceptors. Ni/Au electrodes were used for both the *n*-type and the *p*-type electrodes. The diameter of the Ni/Au *p*-type electrode was 600 μm.

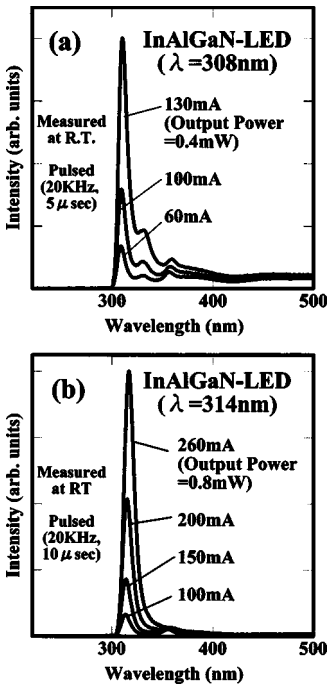

FIG. 20. Electroluminescence (EL) spectra of InAlGaN UV-LEDs with emission wavelengths at (a) 308 and (b) 314 nm for various injection currents measured under RT pulsed operation.

Figures 20(a) and 20(b) show the EL spectra of the UV-LEDs with 308- and 314-nm InAlGaN emitting layers, respectively, as obtained for various injection currents measured under pulsed current injection at RT. We obtained single-peaked emission for both the 308- and 314-nm LEDs. The emission peak was confirmed to originate from the quaternary InAlGaN emitting layer, since the EL peak was just matched to the PL peak. The output power radiated into the backside of the LED was measured using a 10×10-mm Si photodetector located behind the LED sample. The maximum output power was 0.4 mW for 308-nm emission at an injection current of 130 mA, and 0.8 mW for 314-nm emission at an injection current of 260 mA. The external quantum efficiency (EQE) was approximately 0.08% for both LEDs at around maximum output power. The reason for the low efficiency of the LEDs is thought to be the use of bulk InAlGaN for the emitting region. Much higher efficiency might be obtained by using quaternary InAlGaN-based QWs as the active region.

C. 350-nm-band high-power InAlGaN QW LEDs

In this subsection, we describe the fabrication of high-efficiency 350-nm-band UV-LEDs with quaternary InAlGaN MQWs as emitting regions. The LED structures were grown on low-TDD GaN substrates[75,76] and GaN/sapphire templates.[77]

The reduction of the TDD is of considerable importance for suppressing nonradiative recombination and leakage current, especially for AlGaN-based UV emitters. Low-TDD AlGaN buffers fabricated on GaN substrates have been used

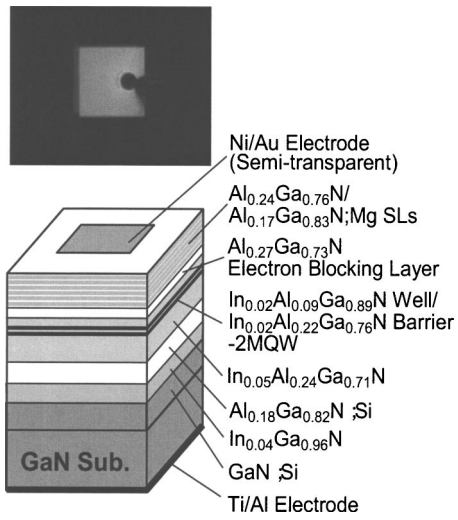

FIG. 21. Schematic structure of a quaternary InAlGaN-based UV-LED fabricated on a GaN substrate and the pattern of the top emission.

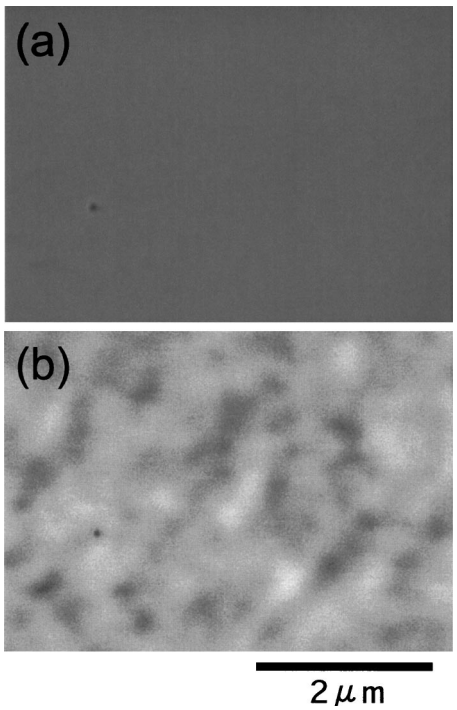

FIG. 22. (a) High-resolution scanning electron microscope (HR-SEM) and (b) cathodoluminescence (CL) images observed on a quaternary InAlGaN MQW layer grown on a GaN substrate.

to achieve high-efficiency UV-LEDs (Ref. 58) or LDs.[109] High-quality GaN substrates have been developed by Sumitomo Electric Industries, Ltd.[110] The advantage of using a quaternary InAlGaN emitter is that UV emission efficiency is less sensitive in comparison with an AlGaN emitter.[70,71] As discussed in Sec. III, the IQE of an InAlGaN-based QW is one to two orders of magnitude larger than that of an AlGaN-based QW when the TDD of the buffer is around 1×10^{10} cm^{-2}. The combination of quaternary InAlGaN active layers and low-TDD buffers is therefore considered to be most effective in realizing 300-350-nm-band high-efficiency UV emitters.[76] In this work, we fabricated quaternary InAlGaN-based UV-LEDs on GaN substrates and GaN/sapphire templates.

The structures were grown at 76 Torr on GaN substrates by MOVPE. High-quality GaN substrates were produced by hydride vapor phase epitaxy by Sumitomo Electric Industries, Ltd.[110] The dislocation density of the GaN substrates was less than 1×10^{6} cm^{-2}. The detailed growth conditions used for the growth of the AlGaN and the quaternary InAlGaN are indicated in the preceding sections.

Figure 21 shows a schematic of the typical structure of an UV-LED fabricated on a GaN substrate and the pattern of the top emission. The structure consists of a 90-nm-thick Si-doped GaN layer deposited directly onto a GaN substrate, an approximately 50-nm-thick undoped $In_{0.04}Ga_{0.96}N$ layer, a 30-nm-thick Si-doped $Al_{0.18}Ga_{0.82}N$ buffer layer, a 35-nm-thick undoped quaternary $In_{0.05}Al_{0.24}Ga_{0.71}N$ buffer layer, an undoped $In_{0.02}Al_{0.09}Ga_{0.89}N/In_{0.02}Al_{0.22}Ga_{0.76}N$ two-layer MQW active region, a 25-nm-thick undoped $Al_{0.27}Ga_{0.73}N$ electron-blocking layer, and a Mg-doped 4-nm-thick $Al_{0.24}Ga_{0.76}N$/4-nm-thick $Al_{0.17}Ga_{0.83}N$ superlattice (SL). The thicknesses of the well and barrier layers of the MQW were approximately 2.5 and 15 nm, respectively. The compositions of the In and Al incorporated in the quaternary InAlGaN were estimated from RBS measurements. We fabricated two types of LEDs, i.e., with *p*-AlGaN/AlGaN SLs and with bulk *p*-$Al_{0.18}Ga_{0.82}N$ layers. The total thickness of the *p*-AlGaN layer was 66 nm in both cases. A 50-nm-thick InGaN layer was inserted just above the Si-doped GaN layer in order to suppress cracks. The samples were annealed at 830 °C in a nitrogen atmosphere at 760 Torr for 50 min in order to activate the Mg acceptors. Then, a Ni/Au semitransparent electrode and a Ti/Al electrode were formed on the *p*-side surface and on the *n*-type GaN substrate, respectively. The size of the *p* electrode was 400×400 μm.[2] The UV output power was detected from the *p* side through the Ni/Au semitransparent electrode. We formed the *p* electrode directly on the *p*-AlGaN layer to reduce the absorption loss. A significant increase in the EQE is expected by the combinational introduction of a QW active region and *p*-AlGaN/AlGaN SLs. The internal quantum efficiency (IQE) of the emitting region could be made more than one order of magnitude larger compared with a bulk emitting region by introducing a QW. This is due to a quantized confinement effect,[71,89] as shown in Figs. 17(a) and 19. Moreover, the hole concentration in the *p* layer would be drastically increased due to a decrease in the equivalent Mg-accepter activation energy[102,103] which is induced by a large piezoelectric field spontaneously applied in AlGaN SLs. The increase in the hole concentration in the *p* layer leads to a significant suppression of electron overflow and the attainment of high electron injection efficiency (EIE), as discussed in Fig. 28.

Figure 22 shows (a) high-resolution scanning electron microscope (HR-SEM) and (b) cathodoluminescence (CL) images observed for a quaternary InAlGaN MQW layer grown on a GaN substrate. In Figs. 22(a) and 22(b), respectively, we can see a small pit and a dark spot, the origin of which is in the threading dislocation (TD).[96,111] The TDD was estimated from 10×13-μm^2 area HR-SEM views, and

was determined to be as low as 1×10^7 cm^{-2}. Emission fluctuations due to In segregation are clearly seen in the CL image, and are considered to contribute to achieve a high-efficiency emission. We have already observed In segregation in quaternary InAlGaN deposited on a high-TDD ($>10^{10}$ cm^{-2}) AlGaN buffer layer.[70] The confirmation that In segregation even occurs in dislocation-free quaternary InAlGaN is found in Fig. 22(b). We did not observe any change in the CL mapping by scanning the detection wavelength.

Figure 23 shows the *I–V* curve and Fig. 24 shows the electroluminescence (EL) spectrum under RT cw operation of an UV-LED fabricated on a GaN substrate. The applied voltage was 4.4 V for an injection current of 100 mA. Single-peaked emission was observed under RT cw operation. The emission wavelengths of a LED with a *p*-AlGaN/AlGaN SL and with a bulk *p*-AlGaN layer were 351.7 and 352.2 nm, respectively. The typical value of the full width at half maximum (FWHM) of the EL emission was 9 nm.

Figure 25 shows the *I–L* characteristics of UV-LEDs fabricated with *p*-AlGaN/AlGaN SLs and with *q* bulk *p*-AlGaN layer under RT cw operation. The maximum UV output power was 7.4 mW for an injection current of 400 mA. The output power was 1.9 mW at an injection current of 50 mA, which is higher than the value of 1.5 mW that has been reported for a 351-nm AlGaN QW LED on a GaN substrate.[58] The wavelength shift of the emission peak due to sample heating was within 0.5 nm, even at a high current injection of 400 mA, indicating that the thermal conductivity of the GaN substrate is sufficiently high.

Figure 26 shows the EQE of the LEDs with the *p*-AlGaN/AlGaN SLs and with a bulk *p*-AlGaN layer under RT cw operation. The maximum EQE obtained for an InAlGaN QW LED with a *p*-AlGaN SL was 1.1% at an injection current of 50 mA, which is obtained for a 350-nm-band UV-LED with top-emission geometry. This value is higher than that obtained for a 351-nm AlGaN QW LED fabricated on a GaN substrate.[58] From these results, the advantages of the use of quaternary InAlGaN in 350-nm-band UV emitters were revealed. The UV output will be further increased by extracting the UV output from the bottom side by removing the GaN substrate or by using a sapphire substrate.

For the efficient operation of UV-LEDs, suppression of the electron overflow into the *p*-AlGaN layer is very important. It would be a problem if the EIE into the QW was significantly reduced by the overflow of electrons. The implementation of a design for obtaining high values of EIE is very important, especially in the case of deep-UV LEDs, since the hole density of the high-Al-content *p*-AlGaN layer is not sufficiently high. Figure 27 shows the *I–L* characteristics of quaternary InAlGaN UV-LEDs fabricated on GaN substrates for various Al contents of the *p*-$Al_xGa_{1-x}N$ electron-blocking layer, measured under RT cw operation. We used an InAlGaN-based three-layer MQW LED structure that emitted at around 358 nm and which was fabricated on a GaN substrate with a bulk *p*-AlGaN layer and a thin *p*-GaN contact layer on the top. The Al contents of 18%, 24%, and 28% used for the of *p*-AlGaN electron-blocking layer in Fig. 27 correspond to electron barrier heights of 0, 80, and 140 meV, respectively. A significant increase in the UV output power was achieved by increasing the Al content of the *p*-$Al_xGa_{1-x}N$ electron-blocking layer. The output power becomes approximately 15 times larger by inserting a *p*-AlGaN electron-blocking layer with a barrier height of 140 meV.

Figure 28 shows the calculated results of the potential distributions of the conduction and the valence bands, the quasi-Fermi levels, the electron- and hole-density distributions, and the electron and hole current densities of InAlGaN three-layer MQW LEDs, with and without an electron-blocking layer. The detailed structure assumed in this analysis is based on the structure used for the experiment in Fig. 27. The thicknesses of the well and barrier layers of the QW were assumed to be 2.5 and 15 nm, respectively. The doping concentrations of the *n*- and *p*-AlGaN layers were assumed to be 1×10^{18} and 2×10^{17} cm^{-3}, respectively. The simulation was performed based on a self-consistent analysis using four equations, i.e., the current-continuity equations and

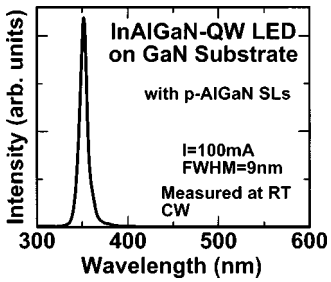

FIG. 24. Electroluminescence (EL) spectrum of a quaternary InAlGaN-based UV-LED on a GaN substrate.

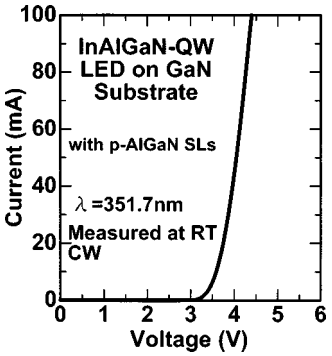

FIG. 23. *I–V* curve of a quaternary InAlGaN-based UV-LED on a GaN substrate.

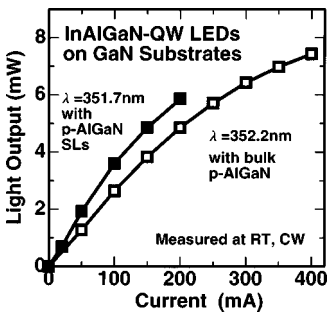

FIG. 25. *I–L* characteristics of InAlGaN-based UV-LEDs fabricated on GaN substrates with *p*-AlGaN/AlGaN SLs and with a bulk *p*-AlGaN layer under RT cw operation.

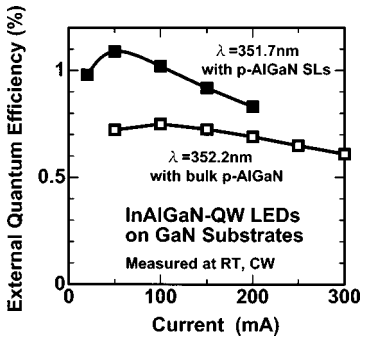

FIG. 26. External quantum efficiency (EQE) of InAlGaN-based UV-LEDs fabricated on GaN substrates with $p-$AlGaN/AlGaN SLs and with a bulk p-AlGaN layer under RT cw operation.

Poisson's equations for the conduction and valence bands.[112,113] We also took into account the continuity condition of the quasi-Fermi levels of the electrons and holes. The values of the electron and hole masses, the effective recombination coefficients, and the electron and hole mobilities of AlGaN and InAlGaN were derived from Refs. 114 and 115. The ratio of the band discontinuity of the conduction and valence bands $\Delta E_c/\Delta E_v$ was assumed to be 2. The barrier height of the electron-blocking layer in the conduction band was assumed to be 150 meV in this calculation.

It can be clearly seen from Fig. 28 that electron overflow into the p-AlGaN layer is effectively blocked by inserting an electron-blocking layer. We can see that the quasi-Fermi level of the electron is sharply bent, and that the electron density in the p-AlGaN layer is significantly reduced by inserting an electron-blocking layer. The electron overflow is reduced to a negligible level due to the reduction of the drift and diffusion currents in the p-AlGaN layer. From the electron and hole current densities in Fig. 28, the values of EIE were calculated to be approximately 99% and 26% for LEDs with and without electron-blocking layers. In the actual devices, the effects of inserting an electron-blocking layer would be even more remarkable because of carrier heating and the effects of feedback due to an increase in nonradiative recombination.

Figure 29 shows a schematic of the structure of an InAlGaN-based MQW UV-LED fabricated on a GaN/sapphire template with p-AlGaN/AlGaN SLs. The thickness of the GaN buffer layer of the GaN/sapphire template was approximately 3 μm. The TDD of the GaN/sapphire template was approximately 1×10^9 cm^{-2}. The LED layer structure deposited on the template is the same as the structure mentioned in Fig. 21. A strong single-peaked emission was observed from the LED under RT cw operation. The emission peak wavelength was 349.1 nm. The FWHM of the EL emission was approximately 9 nm at an injection current of 80 mA.

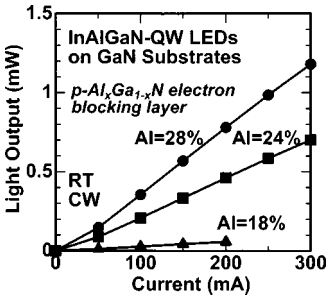

FIG. 27. I–L characteristics of quaternary InAlGaN UV-LEDs on GaN substrates for various Al contents of p-$Al_xGa_{1-x}N$ electron-blocking layer.

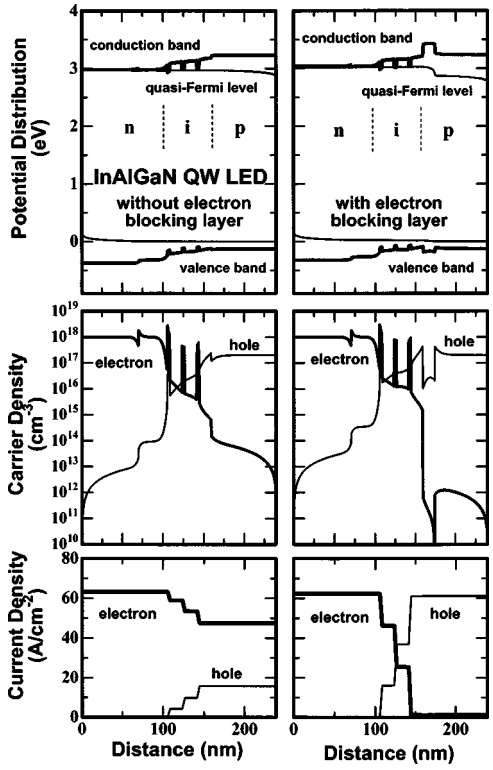

FIG. 28. Calculated results of the potential distributions of the conduction and valence bands, the quasi-Fermi levels, the electron- and hole-density distributions, and the electron and hole current densities of InAlGaN three-layer MQW LEDs with and without an electron-blocking layer.

Figure 30 shows the I–L characteristic of the fabricated InAlGaN-based MQW UV-LED under RT cw operation. The maximum UV output power was 4.1 mW for an injection current of 160 mA. The wavelength shift of the emission peak due to sample heating was 1.6 nm at an injection current of 160 mA, which was larger than that obtained for an InAlGaN-based UV-LED fabricated on a GaN substrate, i.e., 0.5 nm at 400 mA.[75] This indicates that the thermal conductivity of the GaN/sapphire template is not sufficiently high

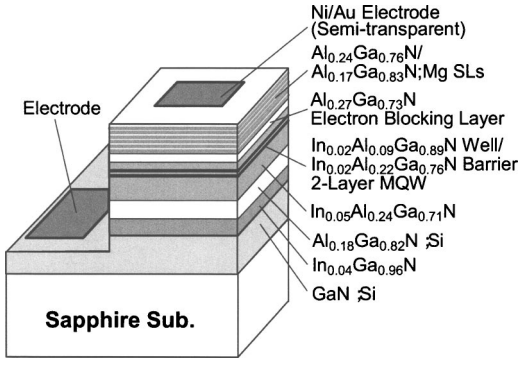

FIG. 29. Schematic structure of a quaternary InAlGaN-based UV-LED fabricated on a GaN/sapphire template.

due to the low thermal conductivity of the sapphire substrate. The output power is saturated when the injection current is above 160 mA. Again, this seems to be caused by the poor thermal conductivity of sapphire substrates in comparison with GaN substrates.

Figure 31 shows the EQE of an InAlGaN-based MQW UV-LED fabricated on a GaN/sapphire template under RT cw operation. The maximum value of EQE was 1.02% with an injection current of 60 mA. This value is as high as that obtained for a 351-nm AlGaN-QW LED fabricated on a GaN substrate.[58] If a high-TDD ($>10^9$ cm^{-2}) GaN or AlGaN template on a sapphire or a SiC substrate is used, the efficiency of the AlGaN-based LED is quite low because the emission intensity of the AlGaN-QW is very sensitive to the TDD, as shown in Ref. 67. On the other hand, high-efficiency emission can be obtained for an InAlGaN-based UV-LED, even when fabricated on a high-TDD template buffer on a sapphire substrate. Therefore, the adoption of quaternary InAlGaN is considered to be very attractive for use in low-cost UV-LEDs for future white-lighting applications. Based on these observations, the advantages of using quaternary InAlGaN in 350-nm-band UV emitters compared with the use of AlGaN are clearly revealed.

The UV output could be further increased by extracting the UV output from the bottom side using a transparent AlGaN/sapphire template. It has been reported that the extraction efficiency of UV light becomes six times larger when it is extracted from the bottom side through a transparent template buffer.[62] Also, the output power will be significantly increased by using a flip-chip structure or by introducing direct wafer bonding and a lift-off process[11] in order to eliminate the effects of sample heating. By using these techniques, the output power of quaternary InAlGaN LEDs could become more than ten times higher.

To summarize this subsection, we demonstrated 350-nm-band high-efficiency UV-LEDs with quaternary InAlGaN MQW emitting regions fabricated on low-TDD GaN substrates and on GaN/sapphire templates. For the LEDs on GaN substrates, the maximum UV output power was 7.4 mW under RT cw operation. The maximum EQE was 1.1%, which is obtained for 350-nm-band UV-LEDs with top-emission geometry. For the LEDs on GaN/sapphire templates, the maximum UV output power was 4.1 mW under RT cw operation. The maximum EQE was 1.02%. From these results, the advantages of using quaternary InAlGaN in 350-nm-band UV emitters in comparison with the use of AlGaN were clearly revealed.

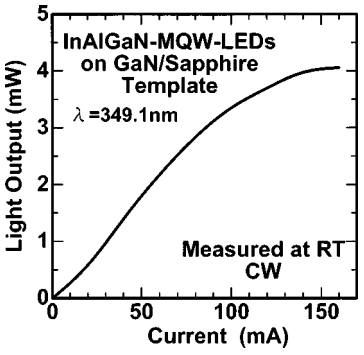

FIG. 30. *I–L* characteristic of an InAlGaN-based UV-LED fabricated on a GaN/sapphire template under RT cw operation.

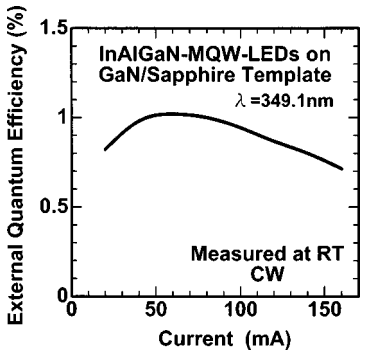

FIG. 31. External quantum efficiency (EQE) of an InAlGaN-based UV-LED fabricated on a GaN/sapphire template under RT cw operation.

V. SUMMARIES AND FUTURE DEVELOPMENTS

We have described techniques for the realization of high-efficiency 300-350-nm-band UV-LEDs by using quaternary InAlGaN emitting layers. We revealed that it is quite effective to use the In-segregation effect that is observed in quaternary InAlGaN to achieve high-efficiency 300-nm-band UV emission. We have demonstrated high-efficiency UV emission from quaternary InAlGaN-based QWs in the wavelength range between 290 and 375 nm at RT by using the In-segregation effect. Emission fluctuations in the submicron region due to In compositional fluctuations were clearly observed for quaternary InAlGaN epitaxial layers. An IQE as high as 15% was estimated for a quaternary InAlGaN-based single quantum well (SQW) at RT. Such high-efficiency UV emission can even be obtained on high threading-dislocation density buffer layers. We also revealed that an alternating gas flow growth technique is useful for obtaining high-Al-content *p*-type AlGaN. Using these techniques, we fabricated 310-nm-band UV-LEDs with quaternary InAlGaN active regions. We achieved submilliwatt output power under RT pulsed operation for 308-314-nm LEDs. We also demonstrated high output power from 350-nm-band quaternary InAlGaN-based LEDs fabricated on GaN substrates and on GaN/sapphire templates, both under RT cw operation.

Based on our results, quaternary InAlGaN will be very useful for producing high-efficiency, high-power UV-LEDs fabricated on low-cost sapphire substrates with emission wavelengths between 290 and 380 nm. However, the maximum IQE of InAlGaN QWs is still around 15%.[74] Recently, we found more appropriate growth conditions for quaternary InAlGaN by further investigation of growth pressure, V/III ratio, and growth temperature. Moreover, the introduction of the alternating gas supply method in MOCVD (Refs. 78 and 79) will be effective for obtaining high-quality quaternary InAlGaN alloys with high Al composition, mainly due to the suppression of vapor-phase reactions of TMAl, TMGa, and NH_3. We investigated these methods for obtaining high IQE in quaternary InAlGaN-based QWs. We predict that the IQE of InAlGaN QWs will become as high as that of InGaN QWs

(50%–70%), because the main source of their efficient emission properties is believed to be the fluctuations of the In content in the alloy in both cases.

At present, the maximum EQE value of InAlGaN-based LEDs on sapphire substrates is only approximately 1%,[6] as shown in the preceding section. This value seems to be too low to realize practical UV emitting devices. Improvements in the extraction efficiency of UV light are necessary in order to improve the EQE. The main reason for the low extraction efficiency is the absorption of UV light by the thick GaN buffer and by the semitransparent electrode, in the cases of our device structures. The extraction efficiency of UV light would be significantly improved by extracting it from the bottom side through the transparent AlGaN/sapphire template, as discussed in Sec. IV C. It would be also much improved by using a flip-chip structure or by introducing direct wafer-bonding and lift-off processes,[11] due to the elimination of the effects of sample heating. We predict that the output power of quaternary InAlGaN-based LEDs could become more than ten times higher by the adoption of these structures. Based on these considerations, device efficiencies of several tens percent (30%–40%) and subwatt output powers for a single chip could be obtained for 300–350-nm-band quaternary InAlGaN-based LEDs by the combination of these improvements in the IQE of QWs and extraction efficiency in the near future.

On the other hand, in terms of the challenges presented in achieving deep-UV LEDs at wavelengths shorter than 280 nm, it is still difficult to obtain high-efficiency emission at RT. The emission properties at RT of AlGaN- and GaN-based QWs are very sensitive to TDD, as mentioned in the preceding sections. The maximum EQE of a 280-nm AlGaN QW LED is still below 1% when fabricated on a high-TDD ($>1\times10^{9}$ cm^{-2}) buffer layer, even after introducing the flip-chip structure for high extraction efficiency.[17] The emission intensity of quaternary InAlGaN QWs is also still low at below 280 nm, as mentioned in Sec. III, therefore, we need to use In-free techniques with AlGaN-based structures in the sub-300-nm UV regime. The use of low-TDD and high-quality AlN substrates would solve these problems. By using AlN substrates, we can obtain AlGaN buffer layers suitable for high-efficiency deep-UV LEDs with TDDs of less than 1×10^{6} cm^{-2},[41,46] while at the same time fabricating stress-free and crack-free layers. The growth method based on alternating gas supply is also useful for the growth of high-quality AlN or high-Al-content AlGaN due to the enhancement of migration and the suppression of the vapor-phase reactions of the precursors.[74] Thus, for sub-300-nm emitters, a combination of the use of high-quality AlN substrates and alternating gas supply growth seems to be most important. Another severe problem is the difficulty in obtaining *p*-type conductivity for high-Al-content AlGaN. Hole concentrations as high as 1×10^{18} cm^{-3} have been obtained for Al contents up to 32% by Hall-effect measurement.[116] However, there have been no reports on the successful measurement of hole concentration for *p*-AlGaN with Al contents greater than 40%. We have confirmed *p*-type conductivity by measuring the I-V curves of LEDs with Mg-doped AlGaN with Al contents of 46%–53%;[74] however, the hole concentration of *p*-AlGaN with Al content greater than 50% is estimated to be less than 1×10^{17} cm^{-3} from the depth of the Mg-acceptor level. We consider that doping techniques, such as codoping or molecular doping, are needed to realize sufficient hole densities for higher Al contents. When the hole density in the *p*-type layer is as low as 1×10^{17} cm^{-3}, electron overflow into the *p* layers is considerably increased, as found from the same analysis used in Fig. 28, which leads to a degradation in the device efficiency. From the basis of these facts, we predict that in the near future, efficient (as high as 10%) UV-LEDs with wavelengths between 250 and 300 nm will be possible by fabricating them on low-TDD and high-quality AlN substrates. Nevertheless, it is still difficult to obtain high-efficiency 200–250-nm LEDs due to the problems of electron overflow that are encountered using the present techniques.

In-free structures fabricated on low-TDD AlN substrates will be also useful for UV-LEDs at wavelengths longer than 300 nm, but we consider that InAlGaN-based structures will be more convenient. The main reason of this is that the emission intensity of InAlGaN-based QWs fabricated on high-TDD buffers is stronger than that of AlGaN-based QWs fabricated on low-TDD substrates, as shown in Sec. IV. Also, the use of sapphire substrates will be more advantageous for the commercial production of UV-LEDs since high-quality AlN substrates are still expensive.

In terms of the challenges involved in obtaining short-wavelength UV-LDs, the use of low-TDD substrates or buffer layers is essential for achieving long-lifetime operation. In general, TDD of lower than 10^{5}–10^{6} cm^{-2} is required in order to obtain the lifetimes of more than 10 000 h. High-quality AlN substrates or AlGaN buffers with TDDs of less than 1×10^{6} cm^{-2} are necessary to realize long-lifetime UV-LDs. Quaternary InAlGaN QWs may also be quite useful for achieving low-threshold current 300–360-nm UV-LDs, due to the high-efficiency emission induced by In-segregation effects. A structure consisting of a high-quality AlN substrate and a quaternary InAlGaN-based emitting layer will be appropriate for achieving low-threshold, high-power, and long-lifetime UV-LDs with wavelengths between 300 and 360 nm.

ACKNOWLEDGMENTS

This review would not have been written without the invitation by Professor Hiroshi Ishiwara of Tokyo Institute of Technology (TIT). I am grateful for having received this opportunity to present the resent progress of group-III nitride-based UV emitting devices. I would like to thank Professor Yoshinobu Aoyagi of TIT for a lot of support and useful discussions. I would like to acknowledge Dr. Takao Nakamura, Katsushi Akita, and Takashi Kyono of Sumitomo Electric Industries (SEI) Ltd. for a lot of experimental support to fabricate and evaluate UV-LEDs on GaN and sapphire substrates. I also wish to thank Dr. Koji Ishibashi for many support to perform this research.

[1]See for example, A. Zukauskas, M. S. Shue, and R. Gaska, *Introduction to Solid-State Lighting* (Wiley, NY, 2002), and references therein.
[2]*Introduction to Nitride Semiconductor Blue Lasers and Light-Emitting Diodes*, edited by S. Nakamura and S. F. Chichibu (Taylor and Francis,

London, 2000).
[3]I. Akasaki and M. Hashimoto, Solid State Commun. **5**, 851 (1967).
[4]H. Amano, N. Sawaki, I. Akasaki, and Y. Toyoda, Appl. Phys. Lett. **48**, 353 (1986).
[5]H. Amano, M. Kito, K. Hiramatsu, and I. Akasaki, Jpn. J. Appl. Phys., Part 2 **28**, L2112 (1989).
[6]I. Akasaki, H. Amano, K. Kito, N. Koide, and K. Manabe, Inst. Phys. Conf. Ser. **129**, 851 (1992).
[7]J. Han *et al.*, Appl. Phys. Lett. **73**, 1688 (1998).
[8]J. Han and M. H. Crawford, Proc. SPIE **3419**, 46 (1998).
[9]A. Kinoshita, H. Hirayama, M. Ainoya, A. Hirata, and Y. Aoyagi, Appl. Phys. Lett. **77**, 175 (2000).
[10]T. Nishida, H. Saito, and N. Kobayashi, Appl. Phys. Lett. **78**, 399 (2001).
[11]D. Morita, M. Sano, M. Yamamoto, T. Murayama, S. Nagahama, and T. Mukai, Jpn. J. Appl. Phys., Part 2 **41**, L1434 (2002).
[12]D. Morita *et al.*, Proc. SPIE **5359**, 415 (2004).
[13]V. Adivarahan, W. H. Sun, A. Chitnis, M. Shatalov, S. Wu, H. P. Maruska, and M. Asif Khan, Appl. Phys. Lett. **85**, 2175 (2004).
[14]S. Wu, V. Adivarahan, M. Shatalov, A. Chitnis, W. H. Sun, and M. Asif Khan, Jpn. J. Appl. Phys., Part 2 **43**, L1035 (2004).
[15]V. Adivarahan *et al.*, Appl. Phys. Lett. **85**, 1838 (2004).
[16]V. Adivarahan, S. Wu, J. P. Zhang, A. Chitnis, M. Shatalov, V. Madavilli, R. Gaska, and M. Asif Khan, Appl. Phys. Lett. **84**, 4762 (2004).
[17]W. H. Sun, V. Adivarahan, M. Shatalov, Y. Lee, S. Wu, J. W. Yang, J. P. Zhang, and M. Asif Khan, Jpn. J. Appl. Phys., Part 2, **43**, L1419 (2004).
[18]J. P. Zhang *et al.*, Appl. Phys. Lett. **81**, 4910 (2002).
[19]W. H. Sun *et al.*, Appl. Phys. Lett. **85**, 531 (2004).
[20]V. Adivarahan, J. P. Zhang, A. Chitnis, W. Shuai, J. Sun, R. Pachipulusu, M. Shatalov, and M. Asif Khan, Jpn. J. Appl. Phys., Part 2 **41**, L435 (2002).
[21]M. Asif Khan, Proc. SPIE **4996**, 188 (2003).
[22]J. P. Zhang, S. Wu, S. Rai, V. Madavilli, V. Adivarahan, A. Chitnis, M. Shatalov, and M. Asif Khan, Appl. Phys. Lett. **83**, 3456 (2003).
[23]V. Adivarahan *et al.*, Appl. Phys. Lett. **81**, 3666 (2002).
[24]A. Chitnis *et al.*, Appl. Phys. Lett. **81**, 2938 (2002).
[25]A. Chitnis, J. P. Zhang, V. Adivarahan, M. Shatalov, S. Wu, R. Pachipulusu, V. Madavilli, and M. Asif Khan, Appl. Phys. Lett. **82**, 2565 (2003).
[26]A. Chitnis *et al.*, Jpn. J. Appl. Phys., Part 2 **41**, L450 (2002).
[27]M. Asif Khan *et al.*, Jpn. J. Appl. Phys., Part 2 **40**, L1308 (2001
[28]A. Chitnis *et al.* Jpn. J. Appl. Phys., Part 2 **41**, L320 (2002
[29]V. Adivarahan *et al.*, Appl. Phys. Lett. **79**, 4240 (2001
[30]A. Yasan, R. McClintock, K. Mayes, D. Shiell, L. Gautero, S. R. Darvish, P. Kung, and M. Razeghi, Appl. Phys. Lett. **83**, 4701 (2003
[31]A. Yasan, R. McClintock, K. Mayes, D. Shiell, S. R. Darvish, P. Kung, and M. Razeghi, Proc. SPIE **5359**, 400 (2004
[32]K. Mayes, A. Yasan, R. McClintock, D. Shiell, S. R. Darvish, P. Kung, and M. Razeghi, Appl. Phys. Lett. **84**, 1046 (2004
[33]A. Yasan, R. McClintock, K. Mayes, S. R. Darvish, P. Kung, and M. Razeghi, Appl. Phys. Lett. **81**, 801 (2002
[34]C. Q. Chen, J. P. Zhang, M. E. Gaevski, H. M. Wang, W. H. Sun, R. S. Q. Fareed, J. W. Yang, and M. Asif Khan, Appl. Phys. Lett. **81**, 4916 (2002
[35]J. P. Zhang, M. Asif Khan, W. H. Sun, H. M. Wang, C. Q. Chen, Q. Fareed, E. Kuokstis, and J. W. Yang, Appl. Phys. Lett. **81**, 4391 (2002
[36]H. Wang, J. P. Zhang, C. Q. Chen, Q. Fareed, J. W. Yang, and M. Asif Khan, Appl. Phys. Lett. **81**, 604 (2002
[37]J. P. Zhang, H. Wang, M. E. Gaevski, C. Q. Chen, Q. Fareed, J. W. Yang, G. Simin, and M. Asif Khan, Appl. Phys. Lett. **80**, 3542 (2002
[38]A. Yasan, R. McClintock, K. Mayes, S. R. Darvish, H. Zhang, P. Kung, and M. Razeghi, Appl. Phys. Lett. **81**, 2151 (2002
[39]G. Tamulaitis, I. Yilmaz, M. S. Shur, Q. Fareed, R. Gaska, and M. Asif Khan, Appl. Phys. Lett. **85**, 206 (2004
[40]E. Kuokstis *et al.* Appl. Phys. Lett. **81**, 2755 (2002
[41]R. Gaska *et al.*, Appl. Phys. Lett. **81**, 4658 (2002
[42]T. N. Oder, K. H. Kim, J. Y. Lin, and X. Jiang, Appl. Phys. Lett. **84**, 466 (2004
[43]J. Shakya, K. H. Kim, J. Y. Lin, and X. Jiang, Appl. Phys. Lett. **85**, 142 (2004
[44]R. Gaska, A. Zukauskas, M. S. Shur, and M. Asif Khan, Proc. SPIE **4776**, 82 (2002
[45]E. Radkov, R. Bompiedi, A. M. Srivastava, A. A. Setlur, and C. A. Becker, Proc. SPIE **5187**, 171 (2004
[46]H. S. Venugopalan *et al.*, Proc. SPIE **4996**, 195 (2003
[47]T. Nishida, T. Ban, and N. Kobayashi, Appl. Phys. Lett. **82**, 3817 (2003
[48]T. Nishida and N. Kobayashi, Proc. SPIE **4641**, 68 (2002
[49]M. H. Crawford, J. Han, W. W. Chow, M. A. Banas, J. J. Figiel, L. Zhang, and R. J. Shul, Proc. SPIE **3938**, 13 (2000
[50]T. Mukai, M. Yamada, and S. Nakamura, Jpn. J. Appl. Phys., Part 2 **37**, L1358 (1998
[51]P. D. Floyd, C. L. Chua, D. W. Treat, and D. P. Bour, Proc. SPIE **3628**, 209 (1999
[52]S. Guha and N. A. Bojarczuk, Appl. Phys. Lett. **73**, 1487 (1998
[53]T. H. Jeys, L. Desmarais, E. J. Lynch, and J. R. Ochoa, Proc. SPIE **5071**, 234 (2003
[54]X. A. Cao, S. F. LeBoeuf, M. P. D'Evelyn, S. D. Arthur, J. Kretchmer, C. H. Yan, and Z. H. Yang, Appl. Phys. Lett. **84**, 4313 (2004).
[55]T. M. Katona, T. Margalith, C. Moe, M. C. Schmidt, S. Nakamura, J. S. Speck, and S. P. DenBaars, Proc. SPIE **5187**, 250 (2004).
[56]A. Hanlon, P. M. Pattison, I. F. Kaeding, R. Sharma, P. Fini, and S. Nakamura, Jpn. J. Appl. Phys., Part 2 **42**, L628 (2003).
[57]O. Schoen, H. Protzmann, M. Luenenbuergar, B. Wachtendorf, B. Schoettker, and M. Heuken, Proc. SPIE **4641**, 76 (2002).
[58]T. Nishida, H. Saito, and N. Kobayashi, Appl. Phys. Lett. **79**, 711 (2001).
[59]T. Nishida, H. Saito, and N. Kobayashi, Appl. Phys. Lett. **78**, 3927 (2001).
[60]T. Nishida, N. Kobayashi, and T. Ban, Appl. Phys. Lett. **82**, 1 (2003).
[61]T. Nishida, T. Makimoto, H. Saito, and T. Ban, Appl. Phys. Lett. **84**, 1002 (2004).
[62]T. Nishida, T. Ban, H. Saito, N. Kobayashi, and T. Makimoto, Proc. SPIE **5359**, 387 (2004).
[63]M. Iwaya *et al.*, Phys. Status Solidi A **188**, 117 (2001).
[64]M. Iwaya, S. Takanami, A. Miyazaki, Y. Watanabe, S. Kamiyama, H. Amano, and I. Akasaki, Jpn. J. Appl. Phys., Part 1 **42**, 400 (2003).
[65]H. Hirayama, Y. Enomoto, A. Kinoshita, A. Hirata, and Y. Aoyagi, Workbook of the Tenth International Conference on Metalorganic Vapor Phase Epitaxy (ICOMVPE-X'2000), 2000, p. 349, Fr-A8.
[66]H. Hirayama, K. Matsunaga, and M. Asada, Electron. Lett. **30**, 142 (1994).
[67]H. Hirayama, S. Tanaka, P. Ramvall, and Y. Aoyagi, Appl. Phys. Lett. **72**, 1736 (1998).
[68]Y. Narukawa, Y. Kawakami, M. Funato, Sz. Fujita, Sg. Fujita, and S. Nakamura, Appl. Phys. Lett. **70**, 891 (1997).
[69]S. Chichibu, T. Azuhara, T. Sota, and S. Nakamura, Appl. Phys. Lett. **70**, 2822 (1997).
[70]H. Hirayama, A. Kinoshita, T. Yamabi, Y. Enomoto, A. Hirata, T. Araki, Y. Nanishi, and Y. Aoyagi, Appl. Phys. Lett. **80**, 207 (2002).
[71]H. Hirayama, Y. Enomoto, A. Kinoshita, A. Hirata, and Y. Aoyagi, Appl. Phys. Lett. **80**, 1589 (2002).
[72]H. Hirayama, A. Kinoshita, A. Hirata, and Y. Aoyagi, Phys. Status Solidi A **188**, 83 (2001).
[73]H. Hirayama, A. Kinoshita, A. Hirata, and Y. Aoyagi, Mater. Res. Soc. Symp. Proc. **639**, G2.8 (2001).
[74]H. Hirayama and Y. Aoyagi, Proc. SPIE **5359**, 422 (2004).
[75]H. Hirayama, K. Akita, T. Kyono, T. Nakamura, and K. Ishibashi, Jpn. J. Appl. Phys., Part 2, **43**, L1241 (2004).
[76]K. Akita, T. Nakamura, and H. Hirayama, Jpn. J. Appl. Phys., Part 1, **43**, 8030 (2004).
[77]H. Hirayama, T. Kyono, K. Akita, T. Nakamura, and K. Ishibashi, Phys. Status Solidi C **2**, 2899 (2005).
[78]J. P. Zhang *et al.*, Appl. Phys. Lett. **79**, 925 (2001).
[79]C. Chen, J. W. Yang, M. Ryu, J. P. Zhang, E. Kuokstis, G. Simin, and M. Asif Khan, Jpn. J. Appl. Phys., Part 2 **41**, L1924 (2002).
[80]M. Shatalov *et al.*, Appl. Phys. Lett. **78**, 817 (2001).
[81]G. Tamulaitis *et al.*, Appl. Phys. Lett. **77**, 2136 (2000).
[82]E. Kuokstis, J. Zhang, M. Ryu, J. W. Yang, G. Simin, M. Asif Khan, R. Gaska, and M. S. Shur, Appl. Phys. Lett. **79**, 4375 (2001).
[83]K. Kazlauskas *et al.*, Appl. Phys. Lett. **82**, 4501 (2003).
[84]J. P. Zhang *et al.*, Jpn. J. Appl. Phys., Part 2 **40**, L921 (2001).
[85]H. Teisseyre *et al.*, Appl. Phys. Lett. **82**, 1541 (2003).
[86]P. Lefebvre *et al.*, Phys. Rev. B **66**, 195330 (2002).
[87]S. Guo, M. Pophristic, D. S. Lee, B. Peres, I. T. Ferguson, J. Lee, and M. Osinski, Proc. SPIE **4776**, 18 (2002).
[88]T. Wang, Y. H. Liu, Y. B. Lee, J. P. Ao, J. Bai, and S. Sakai, Appl. Phys. Lett. **81**, 2508 (2002).
[89]S. J. Rosner, E. C. Carr, M. J. Ludowise, G. Girolami, and H. I. Erikson, Appl. Phys. Lett. **70**, 420 (1997).
[90]T. Sugahara *et al.*, Jpn. J. Appl. Phys., Part 2 **37**, L398 (1998).
[91]T. Miyajima *et al.*, Phys. Status Solidi B **228**, 395 (2001).
[92]H. Hirayama, Y. Enomoto, A. Kinoshita, A. Hirata, and Y. Aoyagi, Appl.

Phys. Lett. **80**, 37 (2002).
[93]H. Hirayama, Y. Enomoto, A. Kinoshita, A. Hirata, and Y. Aoyagi, Phys. Status Solidi A **180**, 157 (2000).
[94]H. Hirayama and Y. Aoyagi, Mater. Res. Soc. Symp. Proc. **537**, G3.74 (1999).
[95]H. Hirayama, Y. Enomoto, A. Kinoshita, A. Hirata, and Y. Aoyagi, Mater. Res. Soc. Symp. Proc. **595**, W11.35 (2000).
[96]H. Hirayama, M. Ainoya, A. Kinoshita, A. Hirata, and Y. Aoyagi, Appl. Phys. Lett. **80**, 2057 (2002).
[97]F. Bernardini, V. Fiorentini, and D. Vanderbilt, Phys. Rev. B **56**, R10024 (1997).
[98]S. Chichibu *et al.*, Appl. Phys. Lett. **73**, 496 (1998).
[99]A. Koukitu, Y. Kumagai, and H. Seki, Work book of the Tenth International Conference on Metalorganic Vapor Phase Epitaxy (ICOMVPE-X'2000), 2000, p. 270, We-P39.-
[100]H. Hirayama, A. Kinoshita, M. Ainoya, T. Yamanaka, A. Hirata, and Y. Aoyagi, Inst. Phys. Conf. Ser. **170**, 195 (2001).
[101]A. Kinoshita, H. Hirayama, M. Ainoya, T. Yamabi, A. Hirata, and Y. Aoyagi, Mater. Res. Soc. Symp. Proc. **693**, 671 (2001).
[102]P. Kozodoy, M. Hansen, S. P. DenBaars, and U. K. Mishra, Appl. Phys. Lett. **74**, 3681 (1999).
[103]P. Kozodoy *et al.*, Appl. Phys. Lett. **75**, 2444 (1999).
[104]V. Kuryatkov *et al.*, Appl. Phys. Lett. **83**, 1319 (2003).
[105]K. Kumakura, T. Makimoto, and N. Kobayashi, Jpn. J. Appl. Phys., Part 1 **39**, 2428 (2000).
[106]K. Kumakura, T. Makimoto, and N. Kobayashi, Jpn. J. Appl. Phys., Part 2 **39**, L195 (2000).
[107]H. Hirayama, Y. Enomoto, A. Kinoshita, A. Hirata, and Y. Aoyagi, Mater. Res. Soc. Symp. Proc. **693**, 295 (2001).
[108]S. Iwai, H. Hirayama, and Y. Aoyagi, Mater. Res. Soc. Symp. Proc. **719**, 3 (2002).
[109]S. Nagahama, T. Yanamoto, M. Sano, and T. Mukai, Jpn. J. Appl. Phys., Part 2 **40**, L785 (2001).
[110]K. Motoki *et al.*, Jpn. J. Appl. Phys., Part 2 **40**, L140 (2001).
[111]K. Kagawa, K. Hoributi, N. Kuwano, K. Oki, and K. Hiramatsu, International Workshop on Nitride Semiconductors (IWN-2000), Nagoya, Japan, 24–27 September 2000 (unpublished), PME-25.
[112]H. Hirayama, Y. Miyake, and M. Asada, IEEE J. Quantum Electron. **28**, 68 (1992).
[113]H. Hirayama, J. Yoshida, Y. Miyake, and M. Asada, IEEE J. Quantum Electron. **30**, 54 (1994).
[114]*Gallium Nitride and Related Semiconductors*, edited by J. H. Edgar, S. Strite, I. Alasaki, H. Amano, and C. Wetzel, EMIS Datareviews Series No. 23 (INSPEC, London, 1999).
[115]*Group III Nitrides*, edited by J. H. Edgar EMIS Datareviews Series No. 11 (INSPEC, London, 1994).
[116]T. Obata, H. Hirayama, Y. Aoyagi, and K. Ishibashi, Phys. Status Solidi A **201**, 2803 (2004).